Cyclin CLB2 mRNA localization and protein synthesis link cell cycle progression to bud growth

Anna Maekiniemi[1], Philipp Savakis[2], Jacky L. Snoep[3,4], Markus Seiler[5], Kelly van Rossum[2], David D. van Niekerk[3], Kathi Zarnack[5], Robert H. Singer[1], Evelina Tutucci[1,2,*]

[1] Cell Biology, Albert Einstein College of Medicine, 1300 Morris Park Avenue, 10461 Bronx, NY, USA

[2] Systems Biology Lab, Amsterdam Institute of Molecular and Life Sciences (AIMMS), Vrije Universiteit Amsterdam, Amsterdam, The Netherlands

[3] Department of Biochemistry, University of Stellenbosch, Private Bag X1, Matieland, 7602, South Africa

[4] Department of Molecular Cell Biology, VU University Amsterdam, De Boelelaan 1085, 1081 HV, Amsterdam, The Netherlands

[5] Buchmann Institute for Molecular Life Sciences (BMLS) & Faculty of Biological Sciences, Goethe University Frankfurt, Max-von-Laue-Str. 15, 60438 Frankfurt, Germany

*Corresponding author: Evelina Tutucci evelina.tutucci@vu.nl

Keywords: mRNA localization, localized translation, smFISH, MS2 system, ZIP code, cell cycle, mitosis, *CLB2*, B-type cyclin, fluorescence microscopy

Figures: 7; Supplementary Figures: 7; Movies: 6; Resources table: 1.

Abstract

Clb2 is a conserved mitotic B-type cyclin, the levels of which are finely controlled to drive progression through the cell cycle. While it is known that *CLB2* transcription and Clb2 protein degradation are important for precise control of its expression, it remains unclear whether the synthesis of Clb2 is also regulated. To address whether and how Clb2 expression levels respond to cell growth changes and adapt cell cycle progression, we combined single-cell and single-molecule imaging methods to measure *CLB2* mRNA and protein expression throughout the *Saccharomyces cerevisiae* cell cycle. We found that the *CLB2* mRNA was efficiently localized to the yeast bud as soon as this compartment was formed, but strikingly the Clb2 protein accumulated in the mother nucleus. The *CLB2* mRNA localization in the yeast bud by the She2-3 complex did not control protein localization but rather promoted *CLB2* translation. Moreover, *CLB2* mRNA bud localization and protein synthesis were coupled and dependent on a single secondary structure -a ZIP code- located in the coding sequence. In a *CLB2* ZIP code mutant, mRNA localization was impaired and Clb2 protein synthesis decreased, resulting in changes in cell cycle distribution and increased size of daughter cells at birth. Finally, while in WT cells the Clb2 protein concentration followed bud growth, this relationship was impaired in the ZIP code mutant. We propose that *S. cerevisiae* couples the control of *CLB2* mRNA bud localization and protein synthesis to coordinate cell growth and cell cycle progression. This mechanism extends our knowledge of *CLB2* expression regulation, and constitutes a novel function for mRNA localization.

Introduction

Over the past decades, RNA imaging technologies have revealed that hundreds of mRNAs localize to various subcellular compartments, in organisms ranging from bacteria to multicellular eukaryotes (Das et al., 2021; Kejiou and Palazzo, 2017), suggesting that mRNA trafficking is a conserved and integral part of gene expression regulation. Current studies suggest that the primary role of mRNA trafficking is to control asymmetric protein distribution to sustain local functions such as cell migration and polarity (Das et al., 2021). Even in the single-cell organism *S. cerevisiae*, dozens of mRNAs localize to the endoplasmic reticulum, mitochondria, and the bud (Niessing et al., 2018). The best-characterized localized mRNA is *ASH1*, which is transported to the yeast bud on actin filaments by the She2-She3 complex and the type V myosin motor Myo4 (Bertrand et al., 1998; Böhl et al., 2000; Long et al., 2000, 1997b, 1997a; Niessing et al., 2004; Shen et al., 2009; Takizawa and Vale, 2000). The RNA binding proteins (RBP) Khd1 and Puf6 bind the *ASH1* mRNA and inhibit its translation until the bud-localized kinases Yck1 and CK2 phosphorylate Khd1 and Puf6, releasing the inhibition and allowing local translation to occur (Deng et al., 2008; Gu et al., 2004; Hasegawa et al., 2008; Irie et al., 2002; Paquin et al., 2007; Shahbabian et al., 2014). The Ash1 protein is subsequently asymmetrically segregated into the daughter nucleus, where it controls mating-type switching (Long et al., 1997b; Niessing et al., 2018). An additional kinase-RBP pair, Cbk1-Ssd1, has been shown to localize to the bud (Wanless et al., 2014) and tune the translation of specific mRNAs (Ballou et al., 2021; Bayne et al., 2022; Jansen et al., 2009).

Besides *ASH1*, multiple mRNAs have been shown to interact with the She2-She3-Myo4 complex and to localize to the bud (Shepard et al., 2003). Among these mRNAs is *CLB2*, which encodes a conserved B-type cyclin, interacting with and controlling the substrate specificity of the cyclin-dependent kinase Cdk1 (Amon et al., 1994, 1993; Fitch et al., 1992; Ghiara et al., 1991; Surana et al., 1993, 1991). The Clb2 protein contains two nuclear localization signals and two nuclear export signals (Hood et al., 2001). Most of the protein is found in the nucleus and at spindle pole

bodies (Bailly et al., 2003; Eluère et al., 2007; Hood et al., 2001). However, when the protein is overexpressed or in nuclear import mutants, the Clb2 protein accumulates in the cytoplasm or at the bud neck (Bailly et al., 2003; Eluère et al., 2007; Hood et al., 2001). Clb2-Cdk1 regulates entry and progression through mitosis in a threshold-dependent manner (Coudreuse and Nurse, 2010; Curran et al., 2022; Fitch et al., 1992; Harvey et al., 2011; Novak et al., 2007; Stern and Nurse, 1996), by phosphorylating transcriptional and post-transcriptional regulators (Darieva et al., 2003; Kõivomägi et al., 2011; Örd and Loog, 2019). This triggers a positive feedback loop leading to the transcription of the *CLB2* cluster, a set of 35 genes including *CLB2*, expressed during the G2/M phase transition (Amon et al., 1993; Enserink and Kolodner, 2010; Spellman et al., 1998; Zhu et al., 2000). Aberrant Clb2 expression -depletion or over-expression- results in abnormal mitotic progression and cell size alteration (Fitch et al., 1992; Machu et al., 2014; Surana et al., 1993). To achieve accurate periodic Clb2 expression, cells combine cell-cycle-dependent mRNA synthesis (Maher et al., 1995; Veis et al., 2007), controlled mRNA decay (Trcek et al., 2011), and proteasome-dependent protein degradation (Hotz and Barral, 2014; Visintin and Amon, 2001). The molecular events controlling *CLB2* transcription and protein degradation, as well as Clb2 function during cell cycle progression, are well characterized. However, it remains unclear whether and how cells modulate *CLB2* mRNA translation in response to changes in cell growth, such as bud growth during *S. cerevisiae* mitosis, and how it may be coupled to cell cycle progression. Previous mathematical modelling suggested that *CLB2* mRNA localization and local translation could act as a bud sizer during the G2/M phase checkpoint (Spiesser et al., 2015), but thus far experimental evidence supporting this hypothesis is lacking.

To investigate this unexplored layer of *CLB2* expression regulation, we performed single-cell measurements of *CLB2* mRNA and protein expression throughout the budding yeast cell cycle in fixed and living cells. We combined single-molecule RNA fluorescence *in situ* hybridization (smFISH) (Femino et al., 1998; Raj et al., 2008) and immunofluorescence (IF) (Maekiniemi et al., 2020; Tutucci and Singer, 2020) to detect *CLB2* mRNA and its protein product simultaneously in

individual cells. Furthermore, to study dynamic gene expression changes in living cells, we utilized the MS2 system (MBSV6) optimized to endogenously tag unstable mRNAs in *S. cerevisiae* (Pichon et al., 2020; Tutucci et al., 2018b, 2018c, 2018a), and tagged the Clb2 protein with GFP. Our work shows that *CLB2* mRNAs are efficiently localized in the bud by the She2-She3 complex during the G2/M phase, while the Clb2 protein is found in the mother nucleus. We show that the *CLB2* mRNA has a single ZIP code located in the coding sequence, which is important for both mRNA localization and Clb2 protein synthesis. We found that bud localization stimulated *CLB2* mRNA translation, as in a *CLB2* ZIP code mutant we observed impaired mRNA bud localization and reduced Clb2 protein synthesis, which were partially rescued in a ZIP code rescue strain. Furthermore, we found that the ZIP code mutant showed an increase in bud size at birth and a small cell cycle distribution defect by flow cytometry. Finally, unlike in wild-type (WT) cells, we observed that protein accumulation in the ZIP code mutant did not correlate with bud growth and thus lost the ability to predict size changes occurring in this compartment. Altogether, we propose that yeast cells have evolved a mechanism that couples the control of *CLB2* mRNA bud localization and protein synthesis to regulate Clb2 protein levels in response to bud growth. We suggest that, in coordination with other known mechanisms controlling *CLB2* expression, this mechanism helps cells monitoring bud growth and fine-tune cell cycle progression.

Results

CLB2 mRNAs localize in the bud from S phase to Mitosis

To quantify *CLB2* mRNA expression throughout the *S. cerevisiae* cell cycle, we combined smFISH and IF. To monitor cell cycle progression, nuclear localization of the transcription factor Whi5 was used to classify early G1 phase, while G2 and mitotic cells were identified by staining tubulin (Tub1) and monitoring microtubules stretching between the mother and the daughter mitotic spindles (**Figure 1A**). *CLB2* smFISH revealed that mRNAs are detected from late S phase, when the bud emerges from the mother cell, until the end of anaphase. Quantification of *CLB2* mRNAs showed that mRNAs are found in 60.7% of cells in an unsynchronized population (**Figure S1A**). The expression peak occurred during G2 (average 10.2 ± 5.7 mRNAs/cell) when about 50% of the cells showed an active transcription site (**Figures 1B and 1C**) with on average 2.9 ± 1.5 nascent RNAs per transcription site, comparable to previous studies (Trcek et al., 2011) (**Figure S1B**). Furthermore, in expressing cells, *CLB2* showed Poissonian transcription kinetics typical of constitutive genes (Zenklusen et al., 2008), suggesting that this cell-cycle regulated gene is likely transcribed in a single activation event. From late S phase until anaphase, we observed that *CLB2* mRNAs localize to the bud from the first stages of bud formation. Throughout the budded phases, we measured up to 65.6% of mRNAs in the bud, as compared to the distribution of the non-localized mRNA *MDN1,* where only 17.2% of mRNAs are found in this compartment (**Figures 1B, 1D, S1C and S1D**). *CLB2* mRNA bud localization is independent of the *S. cerevisiae* background since we observed it both in BY4741, used throughout this study, as well as in the W303 background (**Figure S1E**).

CLB2 mRNAs efficiently localize in the bud of living S. cerevisiae cells

To investigate *CLB2* mRNA localization dynamics in living cells, we used an MS2 system optimized for yeast mRNA tagging (MS2 binding sites V6, MBSV6) (Pichon et al., 2020; Tutucci et al., 2018b, 2018c). We inserted 24xMBSV6 in the 3'UTR of the endogenous *CLB2* locus

(**Figure S2A**). To confirm that mRNA tagging with MBSV6 did not alter *CLB2* mRNA expression, unlike with previous MS2 variants (Garcia and Parker, 2015; Haimovich et al., 2016; Tutucci et al., 2018b), we performed two-color smFISH with probes targeting either the coding sequence (CDS) or the MBSV6 loops, to compare the expression of the endogenous and the tagged *CLB2* mRNA. This confirmed that MS2-tagged mRNAs are full-length and correctly localized in the bud (**Figure S2B**). Furthermore, comparable mRNA levels were observed whether the mRNA was MS2-tagged, with or without GFP-tagged MS2 coat protein (MCP-GFP), which is used to detect mRNAs in living cells (**Figure S2C-E**).

To monitor cell cycle progression and bud emergence in living cells, we tagged the bud neck protein Cdc10 endogenously with tdTomato in the *CLB2*-MS2-tagged strain (**Figure 2A**). We performed time-lapse imaging every 2 minutes and measured *CLB2* mRNA expression throughout the cell cycle by acquiring z-stacks encompassing the cell volume (**Video 1**). To reduce perturbations in gene expression due to synchronization protocols (Schlichting, 2019), we quantified *CLB2* mRNA expression in unsynchronized cells, using the bud neck marker expression to compare cells. This revealed that up to 62.9% of *CLB2* mRNAs localized in the bud (**Figures 2B and 2C**), consistent with the smFISH quantifications (**Figure 1E**). Furthermore, mRNAs were degraded before the end of mitosis with a half-life of 3.8 ± 1.4 min, consistent with previous measurements (Trcek et al., 2011), demonstrating that the MS2 system does not affect *CLB2* mRNA stability (**Figures 2B-D and S2F**). Interestingly, imaging of mother-daughter pairs for more than one cell cycle showed that the daughter cell initiated *CLB2* mRNA expression about 20 minutes after the mother (**Figure 2D**). This observation is in line with previous evidence showing that *S. cerevisiae* daughter cells are born significantly smaller than mothers and that cell size control occurring during G1 regulates the entry into the next cell cycle (Ferrezuelo et al., 2012; Johnston et al., 1977; Leitao and Kellogg, 2017).

High frame-rate imaging every 100 ms revealed that, as the bud grows, the number of *CLB2* mRNAs localized in the bud rapidly increases (**Figure 2E and Video 2**). The high concentration

of mRNAs in the bud and their rapid movement in and outside of the focal plane did not allow tracking single mRNA molecules to investigate *CLB2* mRNAs bud localization dynamics. We therefore used mathematical modelling to predict the behavior of *CLB2* mRNA in the bud of an average G2 cell. The parameters included the bud and mother volumes based on our measurements, mRNA counts and decay rates based on smFISH and live imaging experiments and an apparent mRNA diffusion coefficient based on previous measurements performed in eukaryotic cells (Katz et al., 2016) (**Methods**). A fast coefficient of 0.4 $\mu m^2/s$ was previously measured for non-translating mRNAs, and a slower coefficient of 0.1 $\mu m^2/s$ was measured for translating mRNAs (Katz et al., 2016). Interestingly, our model suggested that if we assumed either a slow or a fast apparent mRNA diffusion coefficient of 0.1 $\mu m^2/s$ or 0.4 $\mu m^2/s$, respectively, we did not obtain the expected enrichment of the *CLB2* mRNA in the bud (**Figures S2G and S2H**). To predict the accumulation of about 65% of the mRNA in the bud observed during the G2 phase, the presence of a high-affinity anchoring factor promoting *CLB2* mRNA segregation in the bud had to be included in the simulation (**Figure S2I**). Altogether, these results showed that *CLB2* mRNAs were efficiently transported to the bud in a cell cycle dependent manner and the simulation implied that the mRNA might be anchored via a yet uncharacterized mechanism.

The CLB2 mRNA has a single She2 binding site in the coding sequence and is transported to the bud via the She2-She3 complex

To elucidate the function of *CLB2* mRNA localization, we first characterized the mechanism of *CLB2* mRNA transport. Previous work showed that *CLB2* mRNA is associated with the She2-She3-Myo4 complex and that localization of *CLB2* to the bud likely requires She2 (Shepard et al., 2003). To expand this observation and quantify this phenotype, we performed smFISH-IF throughout the cell cycle for the *CLB2* mRNA in *SHE2* or *SHE3* gene deletion strains to test whether the She2-She3 complex, required for *ASH1* mRNA transport (Bertrand et al., 1998; Böhl et al., 2000; Long et al., 2000, 1997b, 1997a; Niessing et al., 2004; Shen et al., 2009; Takizawa

and Vale, 2000), was also involved in *CLB2* mRNA localization. This revealed that in *Δshe2* and *Δshe3* strains, localization was strongly impaired (**Figures 3A and S3A**) and that during mitosis only up to 24.5% and 23.6% of *CLB2* mRNAs were found in the bud of the *Δshe2* and *Δshe3* strains, respectively (**Figures S3B and S3C**).

As the She2-She3 complex was required for *CLB2* mRNA localization, we hypothesized that the *CLB2* mRNA might possess a ZIP code akin to the *ASH1* ZIP code. Previous work defined the sequence and structure of the (E3) *ASH1* mRNA ZIP code bound by She2 (Chartrand et al., 1999; Edelmann et al., 2017; Gonzalez et al., 1999; Long et al., 1997a). Based on sequence and structure similarity, a pattern search was performed to predict occurrences within the *CLB2* mRNA (**Methods**). We identified one high-confidence She2-binding site in the CDS at position 1111-1145 (**Figures 3B and 3C**). To test the predicted site, we generated a *CLB2* synonymized mutant whereby the CDS was mutagenized at nine bases to destroy the ZIP code structure, while preserving the protein sequence and the codon usage index (*ZIP mut*, **Figures 3D, S3D and S3E**). A pattern search confirmed that the ZIP code was destroyed upon synonymization. smFISH revealed that, in the *CLB2* ZIP code mutant, the *CLB2* mRNA was no longer bud localized (**Figures 3E and 3F**), demonstrating that the identified ZIP code is sufficient to control bud mRNA localization, possibly by recruiting the She proteins. Furthermore, the loss of *CLB2* mRNA localization was not due to the specific mutations introduced, as alternative ZIP code mutants also showed *CLB2* mRNA mis-localization (**Fig S3D and S3F**). To measure *CLB2* mRNA localization, we quantified the mRNA peripheral distribution index (PDI) in budded cells using the RNA Distribution Index Calculator (Stueland et al., 2019) (**Methods**). The PDI measures the location of the mRNA relative to the nucleus and allows for the comparison of the localization of distinct mRNA species. An index value equals 1 for diffusely distributed mRNAs or >1 if the mRNA has a polarized pattern, and <1 if the mRNA is distributed closer to the nucleus (Stueland et al., 2019) (**Figure 3G**). This analysis revealed a PDI of 1.9 ± 0.42 for the *CLB2* mRNA, similar to the index value of the control mRNA *ASH1* (PDI = 2.2 ± 0.43, **Figure 3H**). The PDI value was

significantly reduced for *CLB2* in the *Δshe2* (PDI = 0.5 ± 0.2), *Δshe3* (PDI = 0.4 ± 0.13), and *CLB2* ZIP code mutant strain (PDI = 0.5 ± 0.16) (ANOVA statistical test: $F(4, 185) = 15.74$, $p < 0.0001$), with PDI values similar to the non-localized mRNA *MDN1* (PDI = 0.6 ± 0.18, **Figures 3H and S1B**). Thus, the She2-3 complex is required to transport *CLB2* mRNAs to the bud via a conserved ZIP code sequence.

Lack of CLB2 mRNA localization affects Clb2 protein expression but not protein localization

To elucidate whether *CLB2* mRNA localization influences its expression, we measured *CLB2* mRNA and protein levels in the localization mutants. Using smFISH, we found comparable mature or nascent RNAs counts in the *Δshe2* (5.3 ±5.1 mRNA/cell and 2.7 ±1.1 nascent RNA/transcription site(TS)) or *Δshe3* mutants (5.2 ±6.2 mRNA/cell and 2.7 ±1.3 nascent RNA/TS) compared to WT cells (5.4 ±5.1 mRNA/cell and 2.6 ±1.3 nascent RNA/TS). While we observed a small but significant increase in the *CLB2* ZIP code mutant strain (6.9 ±6.3 mRNA/cell and 3.4 ±1.3 nascent RNA/TS) compared to WT cells (**Figures 4A and 4B**). Furthermore, a western blot of the endogenously myc-tagged Clb2 protein showed that the protein expression in Δ*she2* or Δ*she3* and in the *CLB2* ZIP code mutants was significantly reduced compared to WT cells (**Figures 4C and 4D**). Interestingly, all ZIP code mutants showed reduced Clb2 protein expression regardless of the ZIP code mutation variant, indicating that this region of the *CLB2* mRNA is important to control mRNA localization and protein expression (**Figures S4A and S4B**). In view of the similarity in the mRNA localization and protein expression phenotypes of the three ZIP mutant strains, we continued the characterization of ZIP code mutant 1 (ZIP^1), henceforth called 'ZIP-mutant'. To test whether the decrease in protein expression was due to a change in protein degradation, we performed stability assays by treating WT and localization mutants with the translation inhibitor cycloheximide and measured the protein abundance over time (**Figures 4E, 4F, S4C and S4D**). No significant difference was observed in the stability of the localization

mutants compared to WT cells, suggesting that *CLB2* mRNA localization, rather than mRNA or protein stability, regulated Clb2 protein synthesis.

Finally, we investigated whether mRNA localization affected Clb2 protein localization. To this end, *CLB2* was endogenously tagged with yeast-optimized GFP (yeGFP) in WT and *CLB2* mRNA localization mutants. We observed that Clb2 is predominantly found in the nucleus in all tested strains (**Figure 4G**), as previously reported for WT cells (Bailly et al., 2003; Eluère et al., 2007; Hood et al., 2001). Interestingly, Clb2 was observed in the mother nucleus already during the G2 phase (**Figure 4G**, top panels), when the mRNAs were already localized to the bud (**Figures 1B, 2B and 3A**), showing an uncoupling between *CLB2* mRNA and protein localization. Altogether, these results suggested that *CLB2* mRNA localization did not segregate the Clb2 protein in the daughter cell, unlike Ash1 (Heym and Niessing, 2012; Long et al., 1997b; Niessing et al., 2018), but rather influenced protein levels.

CLB2 mRNA and protein co-localization suggest preferential translation in the bud.

To simultaneously measure *CLB2* mRNAs and protein expression in single cells, we generated a strain where 25 myc tags were inserted at the N-terminus of the endogenous *CLB2* gene (**Figure 5A**). This N-terminal tagging and amplification strategy increased the Clb2 protein signal without affecting growth (**Figures S5A and S5B**). Next, we combined smFISH and IF to simultaneously detect *CLB2* mRNAs and proteins in fixed cells. Moreover, we used IF against tubulin to score the cell cycle phases. This approach showed that the bulk of Clb2 proteins accumulated in the mother (M) nucleus from G2 to mitosis (**Figures 5B and 5C**), at the time when the mRNA was preferentially found in the bud (B) (**Figures 5B and 5D**). This indicated that Clb2 proteins were efficiently localized in the mother nucleus, as observed by live imaging (**Figure 4G**) and as shown previously (Eluère et al., 2007; Hood et al., 2001). In addition, Clb2 protein foci were also found in the bud in close proximity of *CLB2* mRNAs from G2 to mitosis, suggesting that these foci may represent sites of mRNA translation (**Figure 5B**, yellow arrowheads). Quantification of co-

localized single mRNAs and protein foci (within 250 nm, the resolution of our system) revealed that in WT cells, more co-localized mRNA-protein foci were found in the bud than in the mother cell, while in the localization mutant *Δshe2*, mRNA-protein foci were preferentially found in the mother cell where the bulk of mRNAs was distributed (**Figures 5E and 5F**). Furthermore, we found a significant reduction of the percentage of bud-localized mRNAs co-localized with protein foci in *Δshe2* cells compared to WT cells (**Figure 5G**, non-parametric Mann Whitney test, $P<0.0001$), indicating that in localization mutants *CLB2* mRNA translation efficiency may be reduced. It is interesting to note that even in WT cells, only about 25% of the bud-localized mRNAs were found in close proximity to protein foci, suggesting that *CLB2* mRNAs are translated unfrequently, as previously reported (Arava et al., 2003). Altogether, these data suggest that in WT cells, *CLB2* mRNAs were preferentially translated in the bud, where the mRNA was actively transported. Furthermore, in *Δshe2* cells we observed an increase of protein foci in the mother cell relative to the bud (**Figure 5F**), despite protein levels being decreased under these conditions (**Figure 4**), indicating that translation in the mother cell may be less efficient, resulting in reduced Clb2 protein levels in the localization mutants.

Clb2 protein expression was not affected by the translation regulators Puf6, Ssd1, and Khd1

To investigate if *CLB2* translation efficiency was higher in the bud as a result of translation repression prior to localization, we tested if the deletion of the RNA binding proteins Puf6 (Deng et al., 2008; Gu et al., 2004; Shahbabian et al., 2014), Khd1 (Hasegawa et al., 2008; Irie et al., 2002; Paquin et al., 2007) and Ssd1 (Ballou et al., 2021; Bayne et al., 2022; Jansen et al., 2009), previously shown to inhibit translation of bud-localized mRNAs, influenced Clb2 protein levels. A western blot of the endogenously myc-tagged Clb2 protein in *Δssd1, Δkhd1*, and *Δpuf6* strains (**Figures S5C-E**) did not reveal a significant increase in Clb2 protein levels when comparing the mutant strains to WT (ANOVA statistical test: $F(3, 8) = 0.7677$, $p = 0.3$), which we would have expected if these proteins were inhibiting *CLB2* mRNA translation. Additionally, because Khd1 and Puf6 were shown to be important for *ASH1* mRNA localization (Gu et al., 2004; Irie et al.,

2002), we tested *CLB2* mRNA localization in the mutants. smFISH for the *CLB2* mRNA in the *Δssd1, Δkhd1*, and *Δpuf6* strains showed that the mRNA was still localized in the bud at a similar level as WT cells. Altogether, these results indicated that the factors that control *ASH1* mRNA expression were not required to control *CLB2* mRNAs are translation. While other yet unidentified factors may exist, our data suggested the possibility that *CLB2* mRNA might be translated also outside of the bud, albeit at a reduced rate.

CLB2 mRNA ZIP-mutant displayed increased cell size at birth

The results so far showed that absence of *CLB2* mRNA bud localization correlated with reduced protein expression, likely due to decreased mRNA translation. This suggested that *CLB2* mRNA localization may act as a cellular signal reporting on bud growth to the mother nucleus. To test whether the lack of *CLB2* mRNA localization and the decrease in Clb2 protein levels observed in the mutants affected cell size and cell cycle progression, we performed time-lapse fluorescence microscopy. In all strains, the Clb2 protein was tagged with yeGFP while Cdc10 was fused to mCherry to label the bud neck and monitor division time and mother-daughter size relationships. Live imaging revealed that mother cells of the ZIP-mutant strain were larger at budding and at the division time points (**Figures 6A-D, Videos 3-6**). Furthermore, daughter cells of the ZIP-mutant strain were approximately 10.9% larger at birth than WT daughters (**Figures 6B and 6E**). This did not hold for the *Δshe* mutant strains, where there was a slight reduction of mother size at both budding and division in *Δshe2*, while *Δshe3* was indistinguishable from WT (**Figure S6A-F)**. The ZIP-mutant strain added more material during the budded phase than both WT and the *Δshe* mutants (**Figures 6F, 6G, and S6G**). This effect remained after correcting for mother size (**Figure S6H**) indicating a longer duration of the budded phase in the ZIP-mutant. While the median values for the duration of the budded phase in the ZIP-mutant strain and the WT differed by 5 min, there was significant overlap in the distributions (**Figure S6I**) and this effect was overall not significant (p=0.29, one-way ANOVA). Interestingly, there was a small but significant decrease in budded

time duration for *Δshe2* (**Figure S6J**). To investigate whether nuclear Clb2 levels could report bud size we followed individual cells in time. Fluorescence levels peaked about 20 min before division in all strains (**Figures 6I and S6K**). In accordance with reduced Clb2 protein levels (**Figures 4C, 4D and 4G**), the ZIP-mutant strain exhibited overall lower peak fluorescence intensity than WT (**Figure 6I**). Additionally, in WT cells the signal peaked more sharply (**Figure 6I**). During the buildup to the peak (between 75 to 50 min before division) the ZIP-mutant strain exhibited marginally higher fluorescence (**Figure 6I**) but cumulative fluorescence over the cell cycle indicated that neither a slight increase in baseline nor more time spent at intermediate Clb2 levels compensated for the reduction in translation efficiency observed in the ZIP-mutant strain (**Figures 6J and S6I**). To measure if localized translation of *CLB2* mRNA could report bud size, we correlated bud size against nuclear fluorescence of the corresponding mother cell. While nuclear fluorescence tightly predicted bud size in WT and the *Δshe* mutants' (**Figures 6K and S6M**) this effect was significantly more disperse in the ZIP-mutant strain, indicating a loss of communication between the two compartments. Altogether the data suggest that control of *CLB2* mRNA translation in the bud compartment reports bud size (see Discussion).

Adding the CLB2 WT ZIP code to the 3'UTR of the ZIP mutant promotes translation and rescues cell cycle progression.

We have shown that the ZIP code sequence located in the coding region of the *CLB2* mRNA is necessary for mRNA localization to the bud via the She2-3 complex. To test if the mere presence of the ZIP code in the mRNA is enough for efficient localization we reintroduced the ZIP code into the 3'UTR of the ZIP-mutant strain (**Figure 7A**). smFISH uncovered that adding the WT ZIP code to the 3'UTR resulted in a complete rescue of *CLB2* mRNA localization in the bud, comparable to WT levels (**Figure 7B**), demonstrating that the WT ZIP code was both necessary and sufficient for localizing the mRNA. However, Clb2 protein levels were rescued only partially (**Figures 7C and 7D**), suggesting on one hand that the bud promoted Clb2 translation, but also that the ZIP

code structure in the *CLB2* coding sequence increased *CLB2* mRNA translation via a yet unknown mechanism. Finally, we investigated the growth and cell cycle distribution of the localization mutants and the ZIP code rescue strain. To measure the distribution of the three major phases of the cell cycle (G1, S, G2/M), DNA was labelled with propidium iodide and measured by flow cytometry, followed by Gaussian mixed modelling to estimate the three cell cycle subpopulations. This revealed that, while growth rates of the localization mutants were not significantly affected (**Figure S7A**), we observed a modest but significant (two-way Anova, Dunnett's multiple comparison test) increase in the G2/M fraction in the ZIP-mutant but not in the *Δshe* mutants nor the ZIP-mutant rescue strain (**Figures 7E and 7F**). Altogether, our experiments point to a dual function of the *CLB2* mRNA ZIP code motif, promoting both efficient bud localization and translation. For the latter function to take effect, the ZIP motif needs to be located in the coding sequence. Consistent with this observation, in the *Δshe* mutants where the ZIP code is still intact, higher levels of Clb2 protein were observed. In the ZIP-mutant, where both the localization is impaired and the ZIP code is absent, Clb2 protein levels were lowest in bulk populations (**Figures 4C and 4D**) and in individuals across the cell cycle (**Figure 6I**). We also observed an increased G2/M fraction in this mutant, suggesting that the duration of these stages is increased at the expense of G1 (**Figures 7E and 7F**). Altogether, the higher G2/M fraction (**Figures 7E and 7F**) and the larger size at budding and division (**Figures 6B-G**) indicated that control of *CLB2* mRNA localization and translation play a role in regulating Clb2 protein levels, which in turn report translational maturity as well as size of the bud compartment, providing a mechanism to coordinate growth and cell cycle progression during the G2/M phase transition.

Discussion

In this study, we investigated the complete lifecycle of the *CLB2* gene by combining single-cell and single-molecule imaging methods to measure *CLB2* mRNA and protein expression throughout the *S. cerevisiae* cell division cycle.

CLB2 mRNA localization: same transport as the ASH1 mRNA but distinct regulation

We experimentally demonstrated that the She2-She3 complex transported the *CLB2* mRNA to the bud as soon as this compartment was formed (**Figures 1, 2, 3**), and, based on mathematical modeling (**Figure S2**) propose that active mRNA transport needs to be combined with an anchoring mechanism to explain the highly efficient (>60%) transcript localization, although anchoring factors have yet to be identified. Our observations are consistent with previous work showing that the *CLB2* mRNA can be pulled down using the She2, She3 or Myo4 proteins as bait, as well as with imaging data suggesting *CLB2* mRNA localization in the bud (Shepard et al., 2003). The She2-She3 complex localizes the *ASH1* mRNA to the bud, with the She2-mRNA interaction mediated via the E3 *ASH1* ZIP code located in the *ASH1* coding region (Bertrand et al., 1998; Böhl et al., 2000; Long et al., 2000, 1997b, 1997a; Niessing et al., 2004; Shen et al., 2009; Takizawa and Vale, 2000). We identified an element in the coding region of *CLB2* whose secondary structure resembles that of the *ASH1* ZIP code and demonstrated that this element is both necessary and sufficient for transport into the bud compartment, indicating that it constitutes a bona fide She2 binding site. In *ASH1* the ZIP code motif promotes localization irrespective of its position in the transcript (Bertrand et al., 1998; Chartrand et al., 1999; Gonzalez et al., 1999; Long et al., 1997b; Niedner et al., 2014; Olivier et al., 2005). We could confirm this for the case of *CLB2* where moving the ZIP motif to the 3' UTR resulted in a localization pattern indistinguishable from WT (**Figure 7**). While translation of *ASH1* mRNA is tightly regulated by Puf1 and Khd1 we could find no such inhibition of translation for *CLB2* through either of these factors nor through the bud-localized translation regulator Ssd1 (**Figure S5)**, although we cannot exclude regulation via yet unidentified elements. As Ash1 protein activity needs to be confined to the bud where it controls mating type switching, the reverse appears to be true for the Clb2 protein, which accumulates in the nucleus of the mother cell. Thus, while *ASH1* and *CLB2* localization appears to be controlled by the same cellular machinery, their translational regulation is different.

The CLB2 ZIP code is important for both mRNA localization and protein synthesis control

Alteration of the secondary structure of the ZIP motif through synonymized mutation abolished localization and led to reduced Clb2 protein levels. Moving the ZIP motif from the coding sequence to the 3'UTR rescued *CLB2* localization but the protein concentration did not recover to WT levels. In the *Δshe* mutants, localization was abolished, but protein levels did not decrease to the levels of the ZIP mutant strain. This suggested that an intact ZIP structure located within the coding sequence of *CLB2* is required for optimal translation. We therefore propose that the *CLB2* ZIP motif fulfills a dual role – localization to the bud via She2-She3-Myo4 as well as promotion of translation through as yet unidentified factors.

While our data points to a role of *CLB2* mRNA localization to control its translation and not Clb2 protein nuclear localization (**Figure 4**), we cannot exclude that a transient localization of Clb2 in the bud may have spatially-defined functions that contribute to the observed cell cycle phenotypes. Previous work showed that Clb2 can be found also at the bud neck, when overexpressed (Bailly et al., 2003; Hood et al., 2001) or when Clb2 nuclear import is blocked (Eluère et al., 2007) and that forcing the Clb2 protein in the nucleus can lead to detrimental effect on nuclear fission (Yang et al., 2013). Future studies may uncover additional roles for Clb2 in the bud compartment and at the neck.

Lack of CLB2 mRNA localization and reduced protein expression impact coupling between growth and cell cycle

Our data showed that ZIP-mutant cells are larger at birth and at budding (**Figure 6**). While *S. cerevisiae* mainly exerts size control in G1 (Johnston et al., 1977; Talia et al., 2007), experimental observations (Soifer and Barkai, 2014) and mathematical models (Spiesser et al., 2012) suggested a second size control mechanism in G2. In *Schizosaccharomyces pombe* cell size control is mainly realized in G2, likely through the Clb2 homologue Cdc13 (Curran et al., 2022). A mechanism in which localization of the *CLB2* transcript functions as a reporter of bud compartment maturity was explored previously through mathematical models in which translation

efficiency of *CLB2* mRNA is proportional to bud size volume (Spiesser et al., 2015). In these models, G2/M duration is more variable in the absence of mRNA localization. While our data show a significant increase in cell size owing to a greater amount of material added to the bud compartment during G2 (**Figures 6 and S6**), the effect of mislocalized *CLB2* transcript on the duration of the budded phase were small (**Figures 6 and 7**).

These overall small effects on budded phase duration are likely due to the fact that in the ZIP code mutant about 40-50% of the Clb2 protein is still expressed. This might be at the lower edge of the threshold that suffices to drive mitotic entry and progression (Coudreuse and Nurse, 2010; Curran et al., 2022; Fitch et al., 1992; Harvey et al., 2011; Novak et al., 2007; Stern and Nurse, 1996) which would help to put the absence of a clear cell cycle phenotype of the *Δshe* mutants into perspective. In these mutants, protein levels were reduced, yet there is still significant overlap with WT cell levels (**Figure S6**). Regressing bud size on nuclear Clb2 concentration yielded significantly more disperse predictions in the ZIP-mutant strain than in WT or in the *Δshe* mutants. This suggests that *CLB2* mRNA localization and bud translation may be part of a more complex system coupling bud size control and cell division by combining yet unidentified sizers and timing mechanisms (Facchetti et al., 2017).

Altogether, our data suggest that by coupling *CLB2* mRNA bud localization and protein synthesis, cells coordinate cell growth with cell cycle progression by sensing the bud translation capacity via *CLB2* mRNA transport and local translation. We propose that by shuttling back to the mother nucleus, Clb2 protein levels may signal to the mother cell when the bud is ready for mitosis, establishing a biochemical-based communication between distinct subcellular compartments.

Acknowledgments

We thank X. Meng for help with cloning; J. Wiemerink for help with flow cytometry, A. Gerber for discussion and critical reading of the manuscript, W. Li, C. Eliscovich and S. Das for discussion.

This work was supported by NIH grant GM57071 to R.H.S. E.T. was supported by Swiss National Science Foundation Fellowships P2GEP3_155692 and P300PA_164717, as well as by the Vrije Universiteit Amsterdam. We acknowledge financial support from the Department of Science and Technology/National Research Foundation in South Africa, (grant NRF-SARCHI-82813 to J.L.S.) and for grant 116298 (to D.D.v.N.). K.Z. was supported by the Deutsche Forschungsgemeinschaft (DFG) via the Research Unit FOR2333 (ZA 881/3-1).

Author contributions

Conceptualization, E.T.; Methodology, E.T., A.M., P.S., J.L.S., D.D.N. and K.Z.; Formal Analysis, E.T., A.M., J.L.S., M.S., D.D.N. and P.S.; Investigation, E.T., A.M., P.S. and K.R.; Writing – Original Draft, A.M., E.T.; Writing –Review & Editing, E.T., A.M., R.H.S., P.S., K.Z, and J.L.S.; Funding Acquisition, E.T., J.L.S., K.Z. and R.H.S.; Supervision, E.T., and R.H.S.

Declaration of interests

The material in this manuscript (MS2 system V6) is the subject of a patent application to the US Patent and Trademark Office (no. 18242217). It has not been licensed to any corporation, and the authors (R.H.S., E.T.) are the inventors together with Maria Vera Ugalde (McGill University).

Methods

Yeast strains construction

All strains described in this work were derived from the *S. cerevisiae* background BY4741 (MATa; his3Δ1; leu2Δ0; met15Δ0; ura3Δ0). Strains are listed in the Resource Table. Yeast strains (i.e. deletions and taggings) were constructed as detailed in (Tutucci et al., 2018c). *CLB2* was tagged with 24xMBSV6 in the 3' UTR right after the STOP codon. The MBSV6 insert, followed by the kanamycin resistance gene flanked by LoxP sequences, was PCR amplified from plasmid pET264 (see plasmids in Resource Table) with primers OET017 and OET254, each containing about 70 nucleotides of homology sequence for the *CLB2* gene (see Resource Table). The Kanamycin resistance gene was then removed by expressing the CRE recombinase under the control of the *GAL1* promoter (Resource Table, plasmids). Obtained strains were tested by PCR and sequencing as previously described (Tutucci et al., 2018c).

Plasmids construction

The synonymized *CLB2* ZIP code plasmids were generated by Gibson cloning using the NEB Gibson Assembly Cloning kit (#E5510) using oligos and plasmids as indicated in the resource tables. The plasmids were cut using AatII and EcoRI-HF restriction enzymes and the modified *CLB2* inserts were transformed in BY4741 for homologous recombination. The ZIP-code rescue plasmids were generated by inserting the predicted WT She2 binding site sequence (AGCAGATGACTACGATATACAGTCTCGAACTCTTGCC) at the ClaI restriction site 43 nucleotides downstream of the *CLB2* stop codon.

Yeast cell cultures

Agar plates 2% (w/v) made with yeast extract peptone dextrose (YEPD) or drop-out medium lacking leucine (LEU-) with 2% glucose and 6.7 g/L Yeast Nitrogen Base medium (YNB), were used to grow strains from the -80°C stock or for transformations. Yeasts were grown in 6.7 g/L Yeast Nitrogen Base medium (YNB) with 2% glucose and the appropriate amino acids to

complement the strains' auxotrophies. All experiments were performed growing cells in Synthetic Complete (SC), except the experiments in Figure 2 and S2, where cells were grown in Drop-Out media lacking leucine to maintain the expression of the MCP-2xyeGFP plasmid (pET296). Cells were grown at the indicated temperature using constant shaking at 210 rpm. For smFISH, live imaging and flow cytometry, the details of the cell cultures are described below.

smFISH probes design

CLB2 probes were designed using the Stellaris™ Probe Designer by LGC Biosearch Technologies and purchased from Biosearch Technologies. *ASH1, MDN1* and *MBSV6* probes design was previously described in (Tutucci et al., 2018b, 2018c). Probes sequence and fluorophores are provided in the Resource Table.

Single molecule fluorescence in situ hybridization (smFISH)

Single-molecule FISH (smFISH) was performed as follows. Yeast strains were grown overnight at 26°C in synthetic medium with 2% glucose and containing the appropriate amino acids to complement the strain auxotrophies. In the morning, cells were diluted to OD_{600} 0.1 and allowed to grow until OD_{600} 0.3-0.4. Cells were fixed by adding paraformaldehyde (32% solution, EM grade; Electron Microscopy Science #15714) to a final concentration of 4% and gently shaken at room temperature (RT) for 45 minutes. Cells were then washed three times with buffer B (1.2 M sorbitol and 100 mM potassium phosphate buffer pH 7.5) and resuspended in 500 µL of spheroplast buffer (buffer B containing 20 mM VRC (Ribonucleoside–vanadyl complex NEB #S1402S), and 25 U of Lyticase enzyme (Sigma #L2524) per OD of cells (~10^7 cells) for about 7-8 minutes at 30°C. Digested cells were washed once with buffer B and resuspended in 1 mL of buffer B. 150 µL of cells were seeded on 18 mm poly-L-lysine treated coverslips and incubated at 4°C for 30 minutes. Coverslips were washed once with buffer B, gently covered with ice-cold 70% ethanol and stored at -20°C. For hybridization, coverslips were rehydrated by adding 2xSSC at RT twice for 5 minutes. Coverslips were pre-hybridized with a mix containing 10% formamide

(ACROS organics #205821000)/2xSSC, at RT for 30 minutes. For each coverslip, the probe mix (to obtain a final concentration in the hybridization mix of 125 nM) was added to 5 µL of 10 mg/mL *E. coli* tRNA/ ssDNA (1:1) mix and dried with a speed-vac. The dried mix was resuspended in 25 µL of hybridization mix (10% formamide, 2×SSC, 1 mg/ml BSA, 10 mM VRC, 5 mM $NaHPO_4$ pH 7.5) and heated at 95°C for 3 minutes. Cells were then hybridized at 37°C for 3 hours in the dark. Upon hybridization, coverslips were washed twice with pre-hybridization mix for 30 minutes at 37°C, once with 0.1% Triton X-100 in 2xSSC for 10 minutes at RT, once with 1xSSC for 10 minutes at RT and once with PBS 1x for 10 minutes at RT. Coverslips were quickly dipped in 100% ethanol and let dry at RT covered form light. Finally, coverslips were mounted on glass slides using ProLong Gold antifade (4′,6-diamidino-2-phenylindole) DAPI to counterstain the nuclei (Thermofisher, #P36935).

smFISH-IF

smFISH-IF was performed as previously described in(Maekiniemi et al., 2020; Tutucci and Singer, 2020). In brief, smFISH-IF was performed in a similar way as smFISH, described above. After the last 1xPBS wash of the smFISH, IF was performed on the same coverslips. The smFISH was fixed in 4% PFA in PBS for 10 minutes at RT and then washed for 5 min at RT with 1x PBS. The coverslips were blocked with 1xPBS, 0.1% RNAse-free Bovine Serum Albumin for 30 minutes at RT before being incubated with primary antibodies (Thermofisher, mouse anti-tubulin, 1:1000; Sigma mouse monoclonal anti-myc clone 9E10, 1:1000, Covance, mouse monoclonal anti-HA, 1:1000) in 1xPBS, 0.1% RNAse-free Bovine Serum Albumin for 45 minutes. After being washed with 1xPBS for 5 minutes at RT, the coverslips were incubated with the secondary antibody (goat anti-mouse Alexa 647 1:1500, or goat anti-mouse Alexa 488 1:1500) in 1xPBS, 0.1% RNAse-free Bovine Serum Albumin for 45 minutes at RT. Next, the coverslips were washed with 1x PBS three times for 5 minutes to remove excess antibody. Coverslips were dehydrated by dipping them into

100% ethanol and let dry before mounting onto glass slides using ProLong Gold antifade solution with DAPI.

smFISH and smFISH-IF image acquisition and analysis

Images were acquired using an Olympus BX63 wide-field epi-fluorescence microscope with a 100X/1.35NA UPlanApo objective. Samples were visualized using an X-Cite 120 PC lamp (EXFO) and the ORCA-R2 Digital CCD camera (Hamamatsu). Image pixel size: XY, 64.5 nm. Metamorph software (Molecular Devices) was used for acquisition. Z-sections were acquired at 200 nm intervals over an optical range of 8 µm. FISH images were analyzed using FISHQUANT(Mueller et al., 2013, p.). Briefly, after background subtraction, the FISH spots in the cytoplasm were fit to a three-dimensional (3D) Gaussian to determine the coordinates of the mRNAs. The intensity and width of the 3D Gaussian were filtered to exclude nonspecific signal. The average intensity of all the mRNAs was used to determine the intensity of each transcription site.

Quantification of peripheral distribution index

The peripheral distribution index (PDI) was quantified as described in (Stueland et al., 2019). Briefly, the Matlab-based software RDI (RNA dispersion index) calculator was used to calculate the peripheral distribution index for each cell by identifying cellular RNAs and describing their distribution in relation to the nucleus. Prior to analysis with the RDI calculator, the RNA channel was processed using a 3D Laplacian of Gaussian filter of radius=5 and standard deviation=1. The cell and nucleus channels were processed using the brightness/contrast function in ImageJ to enhance the contrast between the object and the background, as advised in (Stueland et al., 2019).

Co-localization analysis

For the co-localization of *CLB2* mRNA and protein foci in Figure 5, the FISH-quant data for the individual molecules were used as x, y, z coordinates and euclidean distances for all protein -

mRNA molecule combinations were calculated in the mother and daughter cells. Protein and mRNA molecules closer than 250 nm were considered to be in a translation complex. Multiple protein molecules can be within 250 nm of a single mRNA molecule, and this would still be considered a single translation complex.

PDE solution for mRNA diffusion

We use a modified diffusion equation at steady state to model the mRNA movement in terms of diffusion of a concentration *c(x,y,z)* in 3 spatial dimensions, and include binding to ribosomes (uniformly spread) leading to the formation of complexes *b(x,y,z)*:

$$0 = D \cdot \nabla^2 c(x,y,z) - k_d \cdot c(x,y,z) + k_p - k_{\mathrm{on}} \cdot c(x,y,z) + k_{\mathrm{off}} \cdot b(x,y,z)$$

$$0 = k_{\mathrm{on}} \cdot c(x,y,z) - k_{\mathrm{off}} \cdot b(x,y,z) - k_d \cdot b(x,y,z)$$

With decay constant $k_d = \mathrm{Ln}(2)/t_{0.5} = \mathrm{Ln}(2)/240\ \mathrm{s}^{-1}$, $k_{on} = 0.25\ (k_{off} + k_d) = 0.0035$ and $k_{off} = 1/90 = 0.011$ chosen to reflect a half-life of 240 s, a 90 s mean lifetime of ribosome-bound complexes, and that approximately 20% of mRNAs appear bound at steady state. In the high-binding scenario k_{on} was increase by a factor of 125. For the numerical implementation, the production constant is represented by a small non-zero spread around the bud centre using a smooth step-function of which the volume integral is normalized to 1:

$$\mathrm{k_p} = \frac{\mathrm{k_{max}} \cdot \mathrm{e^{s \cdot m}}}{\mathrm{e^{m \cdot r}} + \mathrm{e^{s \cdot m}}}$$

For the simulation results shown in Figure S2, the values chosen are $s = 5$ and $m = 10$, and the normalization results in $k_{max} = 0.0019$. Although the exact value of this constant affects the absolute concentration of mRNA it does not affect the ratio of mother to bud RNA. The PDE is solved in three Cartesian coordinates using the FEM implementation in Wolfram Mathematica (Wolfram Research, Inc., Mathematica, Version 12.3.1, Champaign, IL).

Ellipsoid fitting to mother and bud DIC images

Differential interference contrast (DIC) images were analyzed in Mathematica to fit 3D ellipsoids to mother and bud models. X- and y-axes length were measured for the cells and the short axis was used as estimation of the z-axis. The z-axis origin value was aligned with the z-stack images by maximizing the FISH-Quant mRNA and protein point inclusions.

Pattern search to predict ZIP codes and synonymization

To identify potential ZIP codes in the *CLB2* mRNA, we performed a targeted pattern search (Seiler et al., 2024). In the first step, we leniently screened for two nested pairs of inverted repeats with a minimal length of four nucleotides that framed an asymmetric bulge region as found in the E3 ZIP code in the *ASH1* mRNA (Edelmann et al., 2017). We also checked for the presence of a CGA motif and a singular cytosine on the opposite strand with a defined distance of six nucleotides (Olivier et al., 2005). The search was performed on the complete *CLB2* mRNA with 1476 nt of CDS (YPR119W; genomic coordinates: chromosome XVI, 771653-773128, +, genome version S288C; *Saccharomyces* Genome Database, https://www.yeastgenome.org/locus/S000006323). We further added 366 nt 3' UTR and 346 nt 5' UTR as previously determined by (Trcek et al., 2011). In the second step, the minimum free energy (MFE) folds of all initial instances were analyzed using RNAfold with and without including a constraint on the nested pairs of inverted repeats (Lorenz et al., 2016, 2011). Fold prediction was performed at 28°C with 80 nt RNA sequence fragments centered on each instance. Instances were only kept if (i) at least one of inverted repeat pairs was present in the MFE structure without constraints, and (ii) the free energy (ΔG) of the constraint structure did not differ by more than 20% from the MFE structure without constraint. The latter accounts for energetic benefits from interaction with the She2-She3 proteins. The pattern search predicted a single ZIP code at nucleotide positions +1111 to +1145 of the CDS (genomic coordinates: chromosome XVI, 772763-772797, +). Figure 3C displays the predicted fold with constraint using RNAfold of ZIP

code instance plus ±5 nt flanking sequence. Visualization of the predicted structure in dot-bracket notation was generated using VARNA (Darty et al., 2009). Repeating the pattern search described above on the synonymized ZIP code mutant did not retrieve any hits. The complete sequences of the synonymized ZIP code mutant are provided in the Resource Table.

Sample preparation for live yeast fluorescence imaging

Yeast cells were grown at 26°C in synthetic selective medium. Exponentially growing cells (OD_{600} 0.2-0.4) were plated on coated Delta-T dishes (Bioptech 04200417C). The dishes coating was done by incubating with Concanavalin A 1mg/ml (Cayman chemical company) for 10 minutes at RT. Excess liquid was aspirated and dishes were dried at RT. To activate Concanavalin A, dishes were incubated for 10 minutes at RT with a 50 mM $CaCl_2$ 50 mM $MnCl_2$ solution. Excess was removed and dishes dried at RT. Finally, dishes were washed once with ultrapure water (Invitrogen) and completely dried at RT. Cell attachment was performed by gravity for 20 minutes at RT, excess liquid removed and substitution with fresh media. Cells were diluted to OD_{600} 0.1 and grown until OD_{600} 0.3-0.4. before being plated on Concanavalin A coated dish.

Single molecule mRNA live cell fluorescence imaging and image analysis

The two-color simultaneous imaging of mRNAs and the appropriate cellular marker was performed on a modified version of the home-built microscope described in (Tutucci et al., 2018b, 2018c). Briefly, the microscope was built around an IX71 stand (Olympus). For excitation, a 491 nm laser (CalypsoTM, Cobolt) and a 561 nm laser (JiveTM, Cobolt) were combined and controlled by an acoustic-optic tunable filter (AOTF, AOTFnC-400.650-TN, AA Opto-electronic) before coupled into a single mode optical fiber (Qioptiq). The output of the fiber was collimated and delivered through the back port of the microscope and reflected into an Olympus 150x 1.45 N.A. Oil immersion objective lens with a dichroic mirror (zt405/488/561rpc, 2mm substrate, Chroma). The tube lens (180 mm focal length) was removed from the microscope and placed outside of the right port. A triple band notch emission filter (zet405/488/561m) was used to filter the scattered

laser light. A dichroic mirror (T560LPXR, 3mm substrate, Chroma) was used to split the fluorescence onto two precisely aligned EMCCDs (Andor iXon3, Model DU897) mounted on alignment stages (x, y, z, θ- and φ- angle). Emission filters FF03-525/50-25 and FF01-607/70-25 (Semrock) were placed in front of green and red channel cameras, respectively. The two cameras were triggered for exposure with a TTL pulse generated on a DAQ board (Measurement Computing). The microscope was equipped with a piezo stage (ASI) for fast z-stack and a Delta-T incubation system (Bioptech) for live-cell imaging. The microscope (AOTF, DAQ, Stage and Cameras) was automated with the software Metamorph (Molecular Devices). For two-color live-cell imaging, yeast cells were streamed at 50 ms, Z plane was streamed, and z-stacks acquired every 0.5 µm. Single-molecule analysis was done on maximal projected images using Fiji. Maximally projected images were filtered using the Maxican Hat filter (Radius=2) in Fiji. Spots were identified and counted using the spot detection plugin integrated in TrackMate. LoG detector was used for the spot identification, object diameter= 3 and Quality threshold = 2500. Files were exported as csv files and plotted using GraphPad Prism.

Deconvolution algorithm

To reduce imaging artifacts arising from noise and optics of the microscope, we used the Huygens software v3.6, where a Classic Maximum Likelihood Estimation (CMLE) algorithm was applied as a restoration method to deconvolve the images used for protein-mRNA foci co-localization (Figure 5). CMLE assumes the photon noise to be governed by Poisson statistics and optimizes the likelihood of an estimate of an object in the input 3D image while taking the point spread function into consideration. The CMLE deconvolution method was chosen since it is suited for images with low signal-to-noise ratio and to restore point-like objects. The result is a more accurate identification of the location of the object, which in our case is the fluorescently labeled mRNA and protein molecules. The restoration parameters used with the CMLE deconvolution algorithm was 99 iterations, a quality stop criterion of 0.01, and a signal-to-noise ratio of 15.

CLB2 mRNA bud localization quantification in living cells

For the analysis reported in Figure 2E, the ImageJ plugin Labkit (https://imagej.net/Labkit) was manually used to segment cells and RNAs. Segmented cells were used as input for training the deep learning program Stardist in 2 dimensions. Stardist was used to automatically detect and segment cells and single mRNAs from live imaging movie frames (Cell Detection with Star-convex Polygons, https://arxiv.org/pdf/1806.03535.pdf). Cell and RNA segmentation was imported into R using the RImageJROI package. In R, the cell size, number of mRNAs in the bud and the distance of each bud localized mRNA to the periphery was calculated and plotted over time using the R packages Spatial Data and PBSmapping (Bivand et al., 2013). The Stardist segmentations were used to plot the RNAs and the cell's periphery onto the live imaging movie using the FFmpeg wrapper function for the FFmpeg multimedia framework (https://ffmpeg.org/).

Protein extraction and Western blot

Yeast strains were grown overnight at 26°C in yeast extract peptone dextrose (YEPD) medium with 2% glucose. In the morning, cells were diluted to OD_{600} 0.1 and allowed to grow until OD_{600} 0.5-1. Cell lysis was performed by adding 1 ml H_2O with 150 µL of Yex-lysis buffer (1.85 M NaOH, 7.5% 2-mercaptoethanol) to the pellet of 3-5 ODs of cells (~$3x10^7$) and kept 10 minutes on ice. Proteins were precipitated by the addition of 150 µL of TCA 50% for 10 minutes on ice. Cells were pelleted and resuspended in 100 µL of 1X sample buffer (1 M Tris-HCl pH 6.8, 8 M Urea, 20% SDS, 0.5 M EDTA, 1% 2-mercaptoethanol, 0.05% bromophenol blue). Total protein extracts were fractioned on SDS-PAGE and examined by Western blot with mouse anti-myc (Sigma), mouse anti-Pgk1 (Thermofisher). For quantitative Western blot analyses, fluorescent secondary α-Mouse (IRDye 800CW) and α-Rabbit (IRDye 680RD) antibodies were used. The signals were revealed using the LYCOR® scanner and quantified using LITE® Software.

Clb2 protein imaging in live cells

Cells were precultured in liquid SC medium containing 2% glucose (w/v). Exponentially growing cells were transferred to SC medium containing 2% glucose (w/v), solidified with 1.5% low melt agarose in an ibidi u-Slide 4 well sample holder. Cells were imaged at 30°C using a Nikon Ti-eclipse widefield fluorescence microscope equipped with a SOLA 6-LCR-SB light source (Lumencor), an Andor Zyla 5.5 sCMOS camera, and a Plan Apo lambda 100x immersion Oil objective (NA 1.45, refractive index 1.515). Brightfield images were collected with 20 ms exposure at an LED (CooLED) intensity of 7.6. Clb2p-GFP was imaged at 10% sola intensity with 200 ms exposure and 4x4 hardware binning with a 480/40 excitation filter and a 535/50 emission filter and a 505 nm longpass dichroic (Semrock). Cdc10-mCherry was imaged at 10% sola intensity with 100 ms exposure and 4x4 hardware binning with a 570/20 excitation filter and a 610 longpass emission filter and a 600 nm longpass dichroic (Semrock). Images were taken every 5 min in all three channels.

Image processing

Bright-field images were segmented using a Cellpose model and association of objects in subsequent frames (tracking) was achieved with a maximum matching approach. Briefly, a graph was constructed with cell detections as nodes. Edges were drawn between nodes in subsequent frames if the corresponding cells were less than a predefined threshold (200 px) apart. Edges were given weights computed as 1/(node distance) and then the edge set was found that connected each node to exactly one node in the subsequent frame and that minimized the total distance. Bud necks were detected with a unet-based multiclass detector which was trained to recognize background, cytosol, neck outline and neck centers. The training data for the detector was generated through semi-automatic annotation of Cdc10-mCherry fluorescence images using a napari-based custom interactive random forest plugin. Neck centers in different frames pertaining to the same mother-bud pair were associated into tracks using the tracking approach

described above. Lengths of the neck tracks were reported as budded phase duration. Budding frames were determined as the first time-point at which a fluorescent Cdc10-RFP patch could be detected. In some cases, the emergence of a bud as judged from the bright-field image preceded the formation of a detectable fluorescent patch. In these cases, the budding frame was adjusted manually based on the bright-field information. Pixel areas of mother cells in the budding frame were reported as size of the mother compartment at budding. Pixel areas of mother and daughter cell in the first frame after a bona fide neck could be detected were reported as birth sizes of the respective compartments.

Growth curves setup and analysis

Cells were grown overnight at 30°C in SC with 2% glucose. Cells in mid-log phase were spun down, the supernatant was removed and cells were resuspended at a final OD_{600} of about 0.1 in in SC with 2% glucose. In 48-well plates with flat bottom, 400 µL were plated per well. At least 3 well replicates were done per experiment. Cells were grown for the indicated time, at 30°C. OD_{600} measurements were taken every 5 minutes with 700 rpm orbital shaking between time-points using a CLARIOstar® plate reader (BMG Labtech). Growth curves analysis was performed using an adaptation of the R package Growthcurver (Sprouffske and Wagner, 2016) and plotted using the R package ggplot2 (Wickham, 2016), tydiverse (Wickham et al., 2019), RColorBrewer ("RColorBrewer," n.d.), dplyr ("dplyr," n.d.). Growthcurver fits a basic form of the logistic equation to experimental growth curve data. The logistic equation gives the number of cells N_t at time t.

$$N_t = \frac{K}{1 + \left(\frac{K - N_0}{N_0}\right) e^{-rt}}$$

The population size at the beginning of the growth curve is given by N_0. The maximum possible population size in a particular environment, or the carrying capacity, is given by K. The intrinsic growth rate of the population, r, is the growth rate that would occur if there were no restrictions imposed on total population size. The best values of K, r, and N_0 for the growth curve data were

found using the implementation of the non-linear least-squares Levenberg-Marquardt algorithm. The carrying capacity and growth rate values (*K* and *r*) were used to compare the growth dynamics of the strains.

Flow cytometry sample preparation and analysis

Cells were grown overnight at 30°C in SC medium with 2% glucose. In the morning, cells were diluted to OD_{600} 0.1 and were grown to mid-log phase (OD_{600} 0.3-0.4) with constant shaking (200 rpm) at 30°C. When cells had reached mid-log phase, 1 mL of culture was transferred to a 1.5 mL Eppendorf tube and centrifuged for 3 minutes at 3000 rpm. The supernatant was removed and cells were resuspended in 70% ethanol and fixed overnight at 4°C. Cells were washed once with 1xPBS pH 7.4, resuspended in 500 µL of 1xPBS with 1 µL of RNAse A (1 mg/mL) and incubated at 37°C for 2 hours. After incubation, cells were washed with 1 mL of 1xPBS and resuspended in 200 µL of 1xPBS. The resuspended cells were divided into two tubes: 94 µl of cells were supplemented with 6 µL of a 1 mg/mL solution of propidium iodide (PI), obtaining a final concentration of 60 µg/mL PI, while another 100 µL of cells remained unstained as negative control. Both negative control and PI stained cells were incubated in a water bath at 30°C for 1 hour, covered from the light. Cells were then washed 3 times with 1 mL 1xPBS and resuspended in 500 µl of 1xPBS. The cells were analyzed with the Beckman Coulter CytoFLEX S Flow Cytometer (B2-R0-V2-Y2). A 561 nm laser was used to excite the PI stained cells and a band pass filter (610/20 nm) was used to filter the emitted fluorescence. 50'000 cells were collected per sample. Analysis and plotting was performed using R Studio and the following R packages: ggplot2 (Wickham, 2016); tydiverse (Wickham et al., 2019), RColorBrewer ("RColorBrewer," n.d.), dplyr ("dplyr," n.d.), mixtools (Benaglia et al., 2010).

Quantifications and statistical analysis

FISH-quant was used to quantify single mRNA molecules and protein foci in fixed samples. Fiji was used to quantify single mRNA molecules in living cells. GraphPad Prism was used to

calculate the mean and the standard deviation (SD) of all the data and perform statistical analysis. Flow cytometry data, growth curves analysis was performed in R Studio, as detailed in previous paragraphs. For each experiment, the number of biological replicates, the number of cells analyzed (n), statistical analysis applied and significance is indicated in the figure, figure legend or in the main text. Symbols meaning: ns, $P > 0.05$; *, $P \leq 0.05$; **, $P \leq 0.01$; ***, $P \leq 0.001$, ****, $P \leq 0.0001$.

Figure Legends

Figure 1. CLB2 mRNAs localize to the bud in a cell-cycle dependent manner

(A) Schematic of *CLB2* mRNA expression during the cell cycle. Green dots represent *CLB2* mRNAs. The Whi5 protein (cyan) accumulates in the nucleus during early G1. Tubulin (magenta) is a component of microtubules and the mitotic spindle. The bud stage starts during S phase and ends with the formation of the daughter cell. During anaphase, microtubules stretch between the mother and the daughter cell. **(B)** Top panels: MERGE Maximal projections of IF anti-HA (Whi5) (cyan) and DAPI (blue) merged to a single differential interference contrast (DIC) section (grey). Bottom panels: MERGE Maximal projections of *CLB2* mRNA smFISH (green), anti-tubulin IF (magenta) and DAPI (blue) merged to a single DIC section (grey). The corresponding cell cycle phase is indicated on the panels. Scale bars 3 μm. **(C)** smFISH quantifications of *CLB2* mRNA expression during the different cell cycle phases determined using the markers shown in (B). Dots correspond to individual cells (2083 cells, from two replicates). The black bar indicates the average (G1 early= 1.2±1.9; G1 late= 1.2±1.9; S= 3.8±3.0; G2= 10.3±5.7; M= 8.0±6.5 mRNAs/cell mean ± standard deviation (SD)). **(D)** Relative distribution (bud vs mother) of *CLB2* mRNA in WT budded cells based on the smFISH-IF data shown in (B) (S phase= 58.4±5.5, G2 phase= 34.6±0.9, M phase= 34.4±7.2; mean ± SD).

Figure S1. CLB2 mRNAs are localized also in a different S. cerevisiae background unlike a control mRNA

(A) Quantification of *CLB2* mRNA smFISH shown in Figure 1b reported as relative frequency distribution of mature mRNAs per cell. Data from two replicates (n=2083). **(B)** Quantification of *CLB2* nascent RNAs at transcriptions sites (TS) from smFISH shown in Figure 1b reported as relative frequency distribution of nascent RNAs per TS. Data from two replicates (n=2083). **(C)** MDN1 smFISH maximal projection (green), and DAPI merged to a single DIC section (grey). Scale bar 5 μm **(D)** Relative bud vs mother distribution of *MDN1* mRNA in budded cells based

on the smFISH data shown in (B). Data from two replicates (n=2011; 82.9±3.7, mean ± SD). **(E)** smFISH in the *S. cerevisiae* background W303. MERGE Maximal projections of *CLB2* mRNA smFISH (green) and DAPI (blue) merged to a single DIC section (grey). Scale bar 3 µm.

Figure 2. CLB2 mRNA imaging throughout the cell cycle reveals a rapid mRNA accumulation and localization to the bud

(A) Schematic of *CLB2* localization during the cell cycle. The *CLB2* mRNA (green), the bud neck protein Cdc10 is tagged with tdTomato (magenta). **(B)** *CLB2* endogenously tagged with 24xMBSV6 to enable visualization of the mRNA (black) in live cells. The bud neck protein Cdc10-tdTomato is shown in magenta. Cell A is the mother of cell B. Time point from start of acquisition is indicated in the upper left corner of each time frame. Scale bar 3 µm. **(C)** Percentage of *CLB2* mRNAs localized in the bud over time from bud appearance. Error bars indicates mean ±SD **(D)** Number of *CLB2* mRNAs per cell over time in cell A and cell B. **(E) Top.** Snap shots from live cell imaging of *CLB2* mRNA endogenously tagged with 24xMBSV6. Approximate cell outline identified from fluorescent background (dashed blue line). A single Z plane was acquired every 100 ms. Scale bars 3 µm. **Middle.** Average cell area monitored over time in live cells (n=3). A single Z plane was acquired every 100 ms. Pink, purple and green lines represent time points at which the snapshots on top were taken. **Bottom.** Average number of bud localized mRNAs per cell over time as monitored from 3 single cells. Pink, purple and green lines represent the time points at which the snapshots on top were taken.

Figure S2. CLB2 tagging with the MBSV6 reporter recapitulates CLB2 mRNA expression and mathematical modelling predicts the existence of mRNA anchoring factors in the bud

(A) Schematic of *CLB2* locus endogenously tagged with 24xMBSV6 inserted in the 3' UTR after the STOP codon. Dotted lines represent smFISH probe positions targeting the CDS (green) or MBS sequences (magenta). **(B)** Two-color smFISH for cells expressing tagged *CLB2* mRNAs. Top panels (MBSV6), cells expressing the control vector (YcpLac111). Bottom panels

(MBSV6+MCP) cells expressing MCP (YcpLac111 CYC1p-MCP-NLS-2xyeGFP). DIC/MERGE shows the overlap of the DAPI signal in the nucleus (blue), smFISH for the *CLB2* CDS (green) and the MBS (magenta) with the differential interference contrast (DIC) image. Individual fluorescence channels are shown in grayscale. Scale bars 3 µm. **(C)** Quantification of smFISH shown in (B) as well as untagged WT cells, with CDS probes (green plots) or MBS probes (magenta) reported as distribution of mature mRNAs per cell. Mean of three biological replicates, (*CLB2* MBSV6: CLB2 probes n= 864, mean ± SD 4.9 ± 5.9 mRNA/cell; MBSV6 probes n=771, mean ± SD 5.4 ± 6.1 mRNA/cell; *CLB2* MBSV6+MCP: *CLB2* probes n = 723, mean ± SD 4.5± 5.0 mRNA/cell, MBSV6 probes n=977, mean ± SD 4.9±6.1 mRNA/cell; WT cells: *CLB2* probes n = 791, mean ± SD 5.1±5.1 mRNA/cell). Statistical differences were calculated by non-parametric Mann-Whitney test. **(D-E)** Correlation between the number of single CDS and MBSV6 molecules per cell in presence or absence of MCP. Pearson *r* values calculated by combining two independent experiments (n=1908 and n=2284, respectively). **(F)** Average number of *CLB2* mRNA per cell tagged with 24xMBSV6 monitored over time (purple line), grey represents the SD. **(G-I)** Simulation of localization of mRNA particles per nm^3 assuming **(G)** fast diffusion coefficient of 0.4 $\mu m^2/s$, **(H)** slow diffusion coefficient of 0.1 $\mu m^2/s$ and **(I)** slow diffusion coefficient of 0.1 $\mu m^2/s$ in combination with a high-affinity binding factor.

Figure 3. The She2-3 complex and an RNA ZIP code in CLB2 mRNA CDS are required for bud localization.

(A) smFISH-IF in WT, *Δshe2*, and *Δshe3* strains. MERGE Maximal projections of *CLB2* mRNA smFISH (green), anti-tubulin IF (magenta) and DAPI (blue) merged to a single DIC section (grey). The cell cycle phase is indicated on top of the panel. Scale bars 3 µm. **(B)** Schematic of *CLB2* mRNA coding sequence. The blue box represents the ZIP-code at nucleotides 1111-1145 (relative to START codon). **(C)** Predicted secondary structure of ZIP code (blue box) with flanking sequence (nt 1089- 1168). The free energy (ΔG) of the mRNA folding is indicated. **(D)**

Synonymized ZIP-mutant (*ZIP-mut*). Top sequence is *CLB2* WT. Bottom sequence is the synonymized sequence. Mutated nucleotides are indicated in red. Below is the corresponding Clb2 protein amino acid sequence, which is identical for both the WT and synonymized strains. Rare amino acid codons were avoided to maintain the same codon usage frequency = 0.74 for the *CLB2* mRNA sequence. **(E)** smFISH in WT and ZIP code mutant strain. Maximal projections of smFISH with *CLB2* probes (green) and DAPI (blue) and fluorescence images overlapped to a single DIC section (MERGE). Scale bars 3 µm. **(F)** Relative bud vs mother distribution of the *CLB2* mRNA in WT and ZIP code mutant strain based on smFISH-IF data shown in (e). **(G)** Schematic representation of mRNA peripheral distribution index (PDI). Black dots represent mRNA. Blue is the nucleus. A PDI close to 0 indicates that the RNA of interest is localized near the nucleus. A PDI of 1 indicates that the RNA is diffusely dispersed throughout the cell. As the PDI value grows > 1, the polarization of the mRNA increases. **(H)** PDI in WT cells for *ASH1*, *CLB2* and *MDN1* mRNAs and in *Δshe2*, *Δshe3* and ZIP code mutant strains for the *CLB2* mRNA. Index values are calculated from smFISH-IF experiments shown in (e) and Figure S3A. Significant difference between WT and localization mutants tested by ANOVA statistical test: $F(4, 185) = 15.74$, $p < 0.0001$).

Figure S3. CLB2 is not bud localized in the ⍙she mutants and alternative ZIP code mutants

(A) WT, *Δshe2* and *Δshe3* cells: Left panels, MERGE Maximal projections of *CLB2* mRNA smFISH (green), anti-tubulin IF (magenta) and DAPI (blue) merged to a single DIC section (grey). Right panels, MERGE Maximal projections of IF anti-HA (Whi5) (cyan) and DAPI (blue) merged to a single DIC section (grey). Scale bars 5 µm. **(B)** Relative bud vs mother distribution of the *CLB2* mRNA in *Δshe2* budded cells based on the smFISH-IF data shown in Figures 3A and S3A. (S phase= 92.9±0.2, G2 phase= 82.4±7.9, M phase= 75.5±0.7; mean ± SD). **(C)** Relative bud vs mother distribution of the *CLB2* mRNA in *Δshe3* budded cells based on the smFISH-IF data shown in Figure 3A and in Figure S3A. (S phase= 92.44±3.3, G2 phase= 84.0±4.6, M phase=

76.4±1.8; mean ± SD) (S phase= 58.4±5.5, G2 phase= 34.6±0.9, M phase= 34.4±7.2; mean ± SD). **(D)** Synonymized ZIP-mutant variants (ZIP^1, ZIP^2 and ZIP^3) comparison to *CLB2* WT (top sequence). Mutated nucleotides are indicated in red. Below is the corresponding Clb2 protein amino acid sequence, which is identical for both the WT and synonymized strains. **(E)** Table summarizing the codon usage frequency for the sequences of the three ZIP code variants, ZIP^1, ZIP^2 and ZIP^3 compared to the WT ZIP code. mutant strain. **(F)** smFISH in the ZIP code mutant strains ZIP^2 and ZIP^3. Maximal projections of smFISH with *CLB2* probes (green) and DAPI (blue) and fluorescence images overlapped (MERGE). Scale bars 5 μm.

Figure 4. CLB2 mRNA mis-localization affects Clb2 protein expression but not mRNA levels, nor protein stability or localization

(A) smFISH quantifications of *CLB2* mRNA expression in WT and localization mutants. Dots correspond to individual cells, from at least 3 replicates. The black bar indicates the average number of mRNAs/cell in expressing cells (WT n=3035, 5.4±5.1; *Δshe2* n=1787, 5.3±6.2; *Δshe3* n=1827, 5.2±6.2, ZIP code mutant n=667, 6.9±6.3 mRNAs/cell±SD). Statistical analysis: Anova, Dunnet's multiple comparisons test. **(B)** Quantification of nascent *CLB2* RNAs at transcription sites (TS) from smFISH. Dots correspond to individual cells, from at least 3 replicates (WT n=500, 2.6±1.3; *Δshe2* n=162, 2.7±1.1; *Δshe3* n=186, 2.7±1.3, ZIP code mutant n=132, 3.4±1.3 nascent RNAs/TS±SD). Statistical analysis: Anova, Dunnet's multiple comparisons test. **(C)** Western blot analysis using anti-myc antibody against Clb2 protein endogenously tagged with 5 myc tags in WT, *Δshe2*, *Δshe3* and ZIP code mutant cells. First lane is the control untagged strain. Endogenous Pgk1 protein was used as loading control. **(D)** Quantification of western blot in (c). Myc signal normalized to Pgk1 loading control. Protein levels relative to WT indicated. Mean ± SD from 3 replicates. **(E)** Clb2 protein stability assay in WT, *Δshe2* and *Δshe3* cells. Western blot was performed using an anti-myc antibody to target Clb2 protein tagged with 5 myc tags in cells treated with 100 μg/ml cycloheximide for 0, 5, 10, 20, 30, 45 or 60 minutes. Pgk1 was used as

loading control. Error bars indicates mean ± SD. **(F)** Clb2 protein stability assay in WT and ZIP code mutant as done in (E). Western blot was performed in the same way as in (C). Error bars indicate mean ± SD **(G)** Clb2 fused to yeGFP in WT, *Δshe2*, *Δshe3* and ZIP code mutant cells. Maximal projections of Clb2-GFP (green) overlapped to a single DIC section. Scale bars 2 µm.

Figure S4. Multiple ZIP code mutants show a reduction in Clb2 protein expression and CLB2 mRNA mislocalization is not affecting protein stability

(A) Western blot analysis using anti-myc antibody against Clb2 protein endogenously tagged with 5 myc tags in WT, ZIP^{1}, ZIP^{2} and ZIP^{3}. First lane is the control untagged strain. Endogenous Pgk1 protein was used as loading control. **(B)** Quantification of western blot in (A). Myc signal normalized to Pgk1 loading control. Protein levels relative to WT indicated. Mean ± SD from 4 replicates. **(C)** Example of western blot of Clb2 protein stability assay in WT, *Δshe2* and *Δshe3* cells. Western blot was performed using an anti-myc antibody to target Myc-tagged Clb2 protein tagged in cells treated with 100 µg/ml cycloheximide for 0, 5, 10, 20, 30, 45 or 60 minutes. Pgk1 protein was used as loading control. Quantifications are reported in Figure 4E. **(D)** Example of western blot of Clb2 protein stability assay in WT and ZIP code mutant cells. Western blot was performed using an anti-myc antibody to target Clb2 protein tagged with 5 myc tags in cells treated with 100 µg/ml cycloheximide for 0, 5, 10, 20, 30, 45 or 60 minutes. Pgk1 was used as loading control. Quantifications are reported in Figure 4F.

Figure 5. CLB2 mRNA and protein colocalization suggests preferential translation in the bud.

(A) Schematic of the *CLB2* endogenous gene tagging to simultaneously visualize single mRNA by smFISH and Clb2 proteins by IF against the myc tag in fixed cells. 25 myc tags are inserted at the beginning of the *CLB2* CDS, after the ATG. **(B)** smFISH-IF in WT cells. Top panels: MERGE Maximal projections of IF anti-tubulin (cyan) and DAPI (blue) merged to a single DIC section (grey). Second panel row from the top: MERGE Maximal projections of IF anti-myc-Clb2 protein (magenta), *CLB2* mRNA smFISH (green) and DAPI (blue) merged to a single DIC section (grey).

The third and fourth panels from the top are the *CLB2* mRNA smFISH and Clb2 protein IF, respectively. Scale bars 3 μm. **(C)** Quantification of protein foci in WT bud (B) and mother (M) cells from IF experiments shown in (a). Cell cycle classification was performed using tubulin and DAPI as markers. **(D)** Quantification of mRNA in WT bud (B) and mother (M) cells from smFISH experiments shown in (a). Cell cycle classification was performed as in (b). **(E)** smFISH-IF in *Δshe2* cells. Maximal projections of IF anti-myc-Clb2 protein (magenta), *CLB2* mRNA smFISH (green) and DAPI (blue) merged to a single DIC section (grey). Panels description as in (a). Scale bars 2 μm. **(F)** Quantification of *CLB2* mRNA-protein foci found in close proximity (<250 nm) by smFISH-IF experiments performed in bud (B) and mother (M) cells of WT and *Δshe2* cells shown in panels (A) and (D). **(G)** Quantification of bud-localized mRNAs co-localizing with protein foci (<250 nm) in WT and *Δshe2* cells shown in panels (A) and (D). **** indicate a P value < 0.0001 calculated by using the Mann Whitney significance test.

Figure S5. Known translation inhibitors are not involved in regulating Clb2 protein expression

(A) Western blot analysis of *CLB2* Myc tagged strains. Top row is the myc signal. Bottom row is the Pgk1 loading control. First lane is untagged cells. Second and third lanes are the Clb2 protein tagged with 5 and 25 myc tags, respectively. **(B)** Growth curves of strains with Myc-tagged Clb2 protein performed in SC 2% glucose at 26°C. Growth curves are fitted to a logistic curve (red curve). **(C)** Western blot analysis using anti-myc antibody against Clb2 protein tagged with 25 myc tags in WT, *Δssd1, Δkhd1* and *Δpuf6* cells. Pgk1 protein was used as loading control. First lane is untagged cells. **(D)** Quantification of (C). Mutant strain signal is normalized to WT signal. Each color corresponds to one replicate experiment. Black bar indicates mean ± SD (WT= 100; Δssd1= 88.3±15.6; Δkhd1= 98.8±13.5; Δpuf6= 83.9±10.4). **(E)** Merge maximal projections of *CLB2* smFISH (green), DIC (gray), and DAPI (blue) in WT, *Δssd1, Δkhd1* and *Δpuf6* cells. Scale bars 5 μm.

Figure 6. CLB2 mRNA ZIP code mutant displays larger daughter size and loss of communication between mother and bud compartment

(A) Snapshots from Videos 3 (WT) and 6 (ZIP-mutant) at indicated times from live cell imaging of *CLB2* protein endogenously tagged with yeGFP (green) and Cdc10 tagged with mCherry (magenta). Scale bars 5 µm. Arrows point to single yeast cells undergoing budding and birth of the daughter cell. **(B)** ZIP daughters are born at a larger size. Scaled daughter size at birth vs scaled daughter size at division shown for WT and the ZIP-mutant strain. In both strains daughter size weakly correlates with mother size (Pearson correlation WT: 0.32 (N=431), ZIP:0.25, (N=428). Dotted lines indicate median of the data, divided by median of the WT strain (ZIP-mutant mother size at budding: 1.03, daughter size at birth: 1.109). Data shown were pooled from three biological replicates per strain. Boxplots showing mother size at budding, $p=5.8*10^{-4}$ **(C)**, mother size at division, $p=3.5*10^{-5}$ **(D)**, daughter size at division, $p=2.2*10^{-16}$ **(E)**, combined size of mother and daughter at division, $p=1.44*10^{-13}$ **(F)**, size added during budded phase $p=1.19*10^{-12}$ **(G)** time spent in budded phase p=0.293 **(H)**. Individual boxplots show biological replicates, p values reported are from one-way ANOVA. **(I)** Average fluorescence of Clb2-yeGFP of the 10% brightest pixels per cell as a proxy for nuclear fluorescence over time. Traces shown are recorded between budding and division for cells born in during the experiment and are pooled from three biological replicates. **(J)** boxplot showing cumulative fluorescence signal for the trajectories in (I), $p = 4.3*10^{-12}$, one-way ANOVA.

Figure S6: Δshe mutations have minor effects on cell size

(A) Normalized scatter of scaled daughter size at division vs scaled mother size at budding for *Δshe2* n=598, vs WT (n=431) (A), and for *Δshe3,* (n=475) vs WT **(B)**. Boxplots showing mother size at budding **(C)**, WT vs *Δshe2*: $p=1.2*10^{-5}$, WT vs *Δshe3*: p=0.778, mother size at division **(D)** WT vs *Δshe2*: $p=2.69*10^{-5}$, WT vs *Δshe3*: p=0.573, daughter size at division **(E)**, WT vs *Δshe2*: p=0.107, WT vs *Δshe3*: p=0.412, combined size of mother and daughter compartments at division

(F) WT vs *Δshe2*: p=0.035, WT vs *Δshe3*: p=0.410, size added during budded phase **(G)** WT vs *Δshe2*: p=0.042, WT vs *Δshe3*: p=0.109, size added during budded phase, normalized by mother size **(H)**, WT vs zip: $p=1.96*10^{-4}$, WT vs *Δshe2*: $p=6.42*10^{-5}$, WT vs *Δshe3*: p=0.120. Normalized histogram of budded phase duration for WT and ZIP-code mutant **(I)**. Boxplot of time spent in budded phase **(J)**, WT vs *Δshe2*: $p=1.26*10^{-6}$, WT vs *Δshe3*: p=0.067. p values reported are from one-way ANOVA. **(K)** Average fluorescence of Clb2-yeGFP of the 10% brightest pixels per cell as a proxy for nuclear fluorescence over time. Traces shown are recorded between budding and division for cells born in during the experiment and are pooled from three biological replicates. **(L)** boxplots showing the cumulative signal of the trajectories shown in (K) WT vs *Δshe2*: p=0.507, WT vs *Δshe3*: p=0.324.

Figure 7. The CLB2 ZIP code mutant shows a mild cell cycle defect and ZIP code rescue strain partially recovers protein expression and cell cycle progression

(A) Schematic of *CLB2* ZIP code rescue strain. The blue box represents the WT ZIP code inserted 41 nt after the stop codon in the 3'UTR. The Pink box represent the mutated ZIP code at nucleotides 1111-1145 (nucleotide number relative to START codon). **(B)** smFISH in WT, ZIP code mutant and ZIP code rescue strain. Maximal projections of smFISH with *CLB2* probes (green) and DAPI (blue) and fluorescence images overlapped. Scale bars 3 μm. **(C)** Western blot analysis using anti-myc antibody against Clb2 protein endogenously tagged with 5 myc tags in WT, *Δshe2*, *Δshe3*, ZIP code mutant and ZIP code rescue cells. First lane is the control untagged strain. Endogenous Pgk1 protein was used as loading control. **(D)** Quantification of western blot in (c). Myc signal normalized to Pgk1 loading control. Protein levels relative to WT indicated. Mean ± SD from 3-6 replicates. Asterisk represent significance of <0.05 as determined by t-test. **(E)** Cell cycle analysis by DNA content estimation with flow cytometry in in WT, *Δshe2*, *Δshe3*, ZIP code mutant and ZIP code rescue cells. DNA was stained with propidium iodide to measure the G1 and G2/M components, respectively. **(F)** Relative distribution (%) of cells in G1, S and G2/M phase

obtained by performing mixed Gaussian fitting to estimate the three subpopulations. Mean ± SD from 3 experiments. **(G)** Working model for *CLB2* mRNA localization translation in the *S. cerevisiae* bud.

Figure S7. The CLB2 localization mutants do not show significant growth rates changes

(A) Growth curves of WT, *Δshe2*, *Δshe3*, ZIP code mutant and ZIP code rescue cells performed in SC 2% glucose at 30°C. **(B)** Cell cycle analysis by DNA content estimation with flow cytometry in in WT, *Δshe2*, *Δshe3*, ZIP code mutant and ZIP code rescue cells. Representative experiment showing the results of the mixed Gaussian fitting to estimate the three subpopulations, G1 (purple), S (green) and G2/M (yellow).

Supplementary Video Legends

Video 1. CLB2 mRNA imaging in live cells throughout the cell cycle

CLB2 endogenously tagged with 24xMBSV6 to enable visualization of the mRNA (black) in live cells. The bud neck protein Cdc10-tdTomato is shown in magenta. Two-color imaging was performed by acquiring 13 Z-stacks every 0.5 µm, at two-minutes intervals and with exposure time of 50 ms. In video, at each time point, Z-stacks were max-projected. Scale bar 3 µm.

Video 2. CLB2 mRNA imaging in live cells at high frame-rate acquisition

CLB2 endogenously tagged with 24xMBSV6 to enable visualization of the mRNA (black) in live cells. The bud neck protein Cdc10-tdTomato is shown in magenta. One single Z-stack was streamed every 50 ms. Scale bar 2 µm.

Video 3. Clb2 protein imaging in WT cells

CLB2 endogenously tagged with yeGFP to enable visualization of the protein (green) in WT live cells. The bud neck protein mCherry-Cdc10 is shown in magenta. One single Z-stack was acquired every 5 minutes. Clb2p-GFP was imaged with 200 ms exposure, mCherry-Cdc10 was

imaged with 100 ms exposure and brightfield images were collected with 20 ms exposure. Scale bar 5 µm.

Video 4. Clb2 protein imaging in ⊿she2 cells

CLB2 endogenously tagged with yeGFP to enable visualization of the protein (green) in *⊿she2* live cells. The bud neck protein mCherry-Cdc10 is shown in magenta. One single Z-stack was acquired every 5 minutes. Clb2p-GFP was imaged with 200 ms exposure, mCherry-Cdc10 was imaged with 100 ms exposure and brightfield images were collected with 20 ms exposure. Scale bar 5 µm.

Video 5. Clb2 protein imaging in ⊿she3 cells

CLB2 endogenously tagged with yeGFP to enable visualization of the protein (green) in *⊿she3* live cells. The bud neck protein mCherry-Cdc10 is shown in magenta. One single Z-stack was acquired every 5 minutes. Clb2p-GFP was imaged with 200 ms exposure, mCherry-Cdc10 was imaged with 100 ms exposure and brightfield images were collected with 20 ms exposure. Scale bar 5 µm.

Video 6. Clb2 protein imaging in ZIP-code mutant cells

CLB2 endogenously tagged with yeGFP to enable visualization of the protein (green) in ZIP-code mutant live cells. The bud neck protein mCherry-Cdc10 is shown in magenta. One single Z-stack was acquired every 5 minutes. Clb2p-GFP was imaged with 200 ms exposure, mCherry-Cdc10 was imaged with 100 ms exposure and brightfield images were collected with 20 ms exposure. Scale bar 5 µm.

References

Amon, A., Irniger, S., Nasmyth, K., 1994. Closing the cell cycle circle in yeast: G2 cyclin proteolysis initiated at mitosis persists until the activation of G1 cyclins in the next cycle. Cell 77, 1037–50.

Amon, A., Tyers, M., Futcher, B., Nasmyth, K., 1993. Mechanisms that help the yeast cell cycle clock tick: G2 cyclins transcriptionally activate G2 cyclins and repress G1 cyclins. Cell 74, 993–1007. https://doi.org/10.1016/0092-8674(93)90722-3

Arava, Y., Wang, Y., Storey, J.D., Liu, C.L., Brown, P.O., Herschlag, D., 2003. Genome-wide analysis of mRNA translation profiles in Saccharomyces cerevisiae. Proc Natl Acad Sci U S A 100, 3889–3894. https://doi.org/10.1073/pnas.0635171100

Bailly, E., Cabantous, S., Sondaz, D., Bernadac, A., Simon, M.-N., 2003. Differential cellular localization among mitotic cyclins from Saccharomyces cerevisiae: a new role for the axial budding protein Bud3 in targeting Clb2 to the mother-bud neck. Journal of Cell Science 116, 4119–4130. https://doi.org/10.1242/jcs.00706

Ballou, E.R., Cook, A.G., Wallace, E.W.J., 2021. Repeated Evolution of Inactive Pseudonucleases in a Fungal Branch of the Dis3/RNase II Family of Nucleases. Molecular Biology and Evolution 38, 1837–1846. https://doi.org/10.1093/molbev/msaa324

Bayne, R.A., Jayachandran, U., Kasprowicz, A., Bresson, S., Tollervey, D., Wallace, E.W.J., Cook, A.G., 2022. Yeast Ssd1 is a non-enzymatic member of the RNase II family with an alternative RNA recognition site. Nucleic Acids Research 50, 2923–2937. https://doi.org/10.1093/nar/gkab615

Benaglia, T., Chauveau, D., Hunter, D.R., Young, D.S., 2010. mixtools: An R Package for Analyzing Mixture Models. Journal of Statistical Software 32, 1–29. https://doi.org/10.18637/jss.v032.i06

Bertrand, E., Chartrand, P., Schaefer, M., Shenoy, S.M., Singer, R.H., Long, R.M., 1998. Localization of ASH1 mRNA particles in living yeast. Mol Cell 2, 437–45.

Bivand, R.S., Pebesma, E., Gómez-Rubio, V., 2013. Applied Spatial Data Analysis with R, 2nd ed, Use R! Springer-Verlag, New York. https://doi.org/10.1007/978-1-4614-7618-4

Böhl, F., Kruse, C., Frank, A., Ferring, D., Jansen, R.-P., 2000. She2p, a novel RNA-binding protein tethers ASH1 mRNA to the Myo4p myosin motor via She3p. EMBO J 19, 5514–5524. https://doi.org/10.1093/emboj/19.20.5514

Chartrand, P., Meng, X.-H., Singer, R.H., Long, R.M., 1999. Structural elements required for the localization of ASH1 mRNA and of a green fluorescent protein reporter particle in vivo. Current Biology 9, 333–338. https://doi.org/10.1016/S0960-9822(99)80144-4

Coudreuse, D., Nurse, P., 2010. Driving the cell cycle with a minimal CDK control network. Nature 468, 1074–1079. https://doi.org/10.1038/nature09543

Curran, S., Dey, G., Rees, P., Nurse, P., 2022. A quantitative and spatial analysis of cell cycle regulators during the fission yeast cycle. Proc Natl Acad Sci U S A 119, e2206172119. https://doi.org/10.1073/pnas.2206172119

Darieva, Z., Pic-Taylor, A., Boros, J., Spanos, A., Geymonat, M., Reece, R.J., Sedgwick, S.G., Sharrocks, A.D., Morgan, B.A., 2003. Cell cycle-regulated transcription through the FHA domain of Fkh2p and the coactivator Ndd1p. Curr Biol 13, 1740–1745. https://doi.org/10.1016/j.cub.2003.08.053

Darty, K., Denise, A., Ponty, Y., 2009. VARNA: Interactive drawing and editing of the RNA secondary structure. Bioinformatics 25, 1974–1975. https://doi.org/10.1093/bioinformatics/btp250

Das, S., Vera, M., Gandin, V., Singer, R.H., Tutucci, E., 2021. Intracellular mRNA transport and localized translation. Nature Reviews Molecular Cell Biology 1–22. https://doi.org/10.1038/s41580-021-00356-8

Deng, Y., Singer, R.H., Gu, W., 2008. Translation of ASH1 mRNA is repressed by Puf6p-Fun12p/eIF5B interaction and released by CK2 phosphorylation. Genes & development 22, 1037–50. https://doi.org/10.1101/gad.1611308

dplyr: A Grammar of Data Manipulation — dplyr-package [WWW Document], n.d. URL https://dplyr.tidyverse.org/reference/dplyr-package.html (accessed 2.4.22).

Edelmann, F.T., Schlundt, A., Heym, R.G., Jenner, A., Niedner-Boblenz, A., Syed, M.I., Paillart, J.-C., Stehle, R., Janowski, R., Sattler, M., Jansen, R.-P., Niessing, D., 2017. Molecular architecture and dynamics of ASH1 mRNA recognition by its mRNA-transport complex. Nature Structural & Molecular Biology 24, 152–161. https://doi.org/10.1038/nsmb.3351

Eluère, R., Offner, N., Varlet, I., Motteux, O., Signon, L., Picard, A., Bailly, E., Simon, M.-N., 2007. Compartmentalization of the functions and regulation of the mitotic cyclin Clb2 in S. cerevisiae. J Cell Sci 120, 702–711. https://doi.org/10.1242/jcs.03380

Enserink, J.M., Kolodner, R.D., 2010. An overview of Cdk1-controlled targets and processes. Cell Div 5, 11. https://doi.org/10.1186/1747-1028-5-11

Facchetti, G., Chang, F., Howard, M., 2017. Controlling cell size through sizer mechanisms. Curr Opin Syst Biol 5, 86–92. https://doi.org/10.1016/j.coisb.2017.08.010

Femino, A.M., Fay, F.S., Fogarty, K., Singer, R.H., 1998. Visualization of single RNA transcripts in situ. Science 280, 585–90.

Ferrezuelo, F., Colomina, N., Palmisano, A., Garí, E., Gallego, C., Csikász-Nagy, A., Aldea, M., 2012. The critical size is set at a single-cell level by growth rate to attain homeostasis and adaptation. Nat Commun 3, 1012. https://doi.org/10.1038/ncomms2015

Fitch, I., Dahmann, C., Surana, U., Amon, A., Nasmyth, K., Goetsch, L., Byers, B., Futcher, B., 1992. Characterization of four B-type cyclin genes of the budding yeast Saccharomyces cerevisiae. Molecular biology of the cell 3, 805–18.

Garcia, J.F., Parker, R., 2015. MS2 coat proteins bound to yeast mRNAs block 5' to 3' degradation and trap mRNA decay products: implications for the localization of mRNAs by MS2-MCP system. RNA 21, 1393–5. https://doi.org/10.1261/rna.051797.115

Ghiara, J.B., Richardson, H.E., Sugimoto, K., Henze, M., Lew, D.J., Wittenberg, C., Reed, S.I., 1991. A cyclin B homolog in S. cerevisiae: chronic activation of the Cdc28 protein kinase by cyclin prevents exit from mitosis. Cell 65, 163–174. https://doi.org/10.1016/0092-8674(91)90417-w

Gonzalez, I., Buonomo, S.B.C., Nasmyth, K., Ahsen, U. von, 1999. ASH1 mRNA localization in yeast involves multiple secondary structural elementsand Ash1 protein translation. Current Biology 9, 337–340. https://doi.org/10.1016/S0960-9822(99)80145-6

Gu, W., Deng, Y., Zenklusen, D., Singer, R.H., 2004. A new yeast PUF family protein, Puf6p, represses ASH1 mRNA translation and is required for its localization. Genes & development 18, 1452–65. https://doi.org/10.1101/gad.1189004

Haimovich, G., Zabezhinsky, D., Haas, B., Slobodin, B., Purushothaman, P., Fan, L., Levin, J.Z., Nusbaum, C., Gerst, J.E., 2016. Use of the MS2 aptamer and coat protein for RNA localization in yeast: A response to "MS2 coat proteins bound to yeast mRNAs block 5' to 3' degradation and trap mRNA decay products: implications for the localization of mRNAs by MS2-MCP system." RNA 22, 660–6. https://doi.org/10.1261/rna.055095.115

Harvey, S.L., Enciso, G., Dephoure, N., Gygi, S.P., Gunawardena, J., Kellogg, D.R., 2011. A phosphatase threshold sets the level of Cdk1 activity in early mitosis in budding yeast. MBoC 22, 3595–3608. https://doi.org/10.1091/mbc.e11-04-0340

Hasegawa, Y., Irie, K., Gerber, A.P., 2008. Distinct roles for Khd1p in the localization and expression of bud-localized mRNAs in yeast. RNA 14, 2333–2347. https://doi.org/10.1261/rna.1016508

Heym, R.G., Niessing, D., 2012. Principles of mRNA transport in yeast. Cell Mol Life Sci 69, 1843–53. https://doi.org/10.1007/s00018-011-0902-4

Hood, J.K., Hwang, W.W., Silver, P.A., 2001. The Saccharomyces cerevisiae cyclin Clb2p is targeted to multiple subcellular locations by cis- and trans-acting determinants. Journal of Cell Science 114, 589–597.

Hotz, M., Barral, Y., 2014. The Mitotic Exit Network: new turns on old pathways. Trends in Cell Biology 24, 145–152. https://doi.org/10.1016/j.tcb.2013.09.010

Irie, K., Tadauchi, T., Takizawa, P.A., Vale, R.D., Matsumoto, K., Herskowitz, I., 2002. The Khd1 protein, which has three KH RNA-binding motifs, is required for proper localization of ASH1 mRNA in yeast. The EMBO journal 21, 1158–67. https://doi.org/10.1093/emboj/21.5.1158

Jansen, J.M., Wanless, A.G., Seidel, C.W., Weiss, E.L., 2009. Cbk1 Regulation of the RNA-Binding Protein Ssd1 Integrates Cell Fate with Translational Control. Current Biology 19, 2114–2120. https://doi.org/10.1016/j.cub.2009.10.071

Johnston, G.C., Pringle, J.R., Hartwell, L.H., 1977. Coordination of growth with cell division in the yeast Saccharomyces cerevisiae. Experimental cell research 105, 79–98.

Katz, Z.B., English, B.P., Lionnet, T., Yoon, Y.J., Monnier, N., Ovryn, B., Bathe, M., Singer, R.H., 2016. Mapping translation “hot-spots” in live cells by tracking single molecules of mRNA and ribosomes. Elife 5. https://doi.org/10.7554/eLife.10415

Kejiou, N.S., Palazzo, A.F., 2017. mRNA localization as a rheostat to regulate subcellular gene expression. Wiley Interdiscip Rev RNA 8. https://doi.org/10.1002/wrna.1416

Kõivomägi, M., Valk, E., Venta, R., Iofik, A., Lepiku, M., Morgan, D.O., Loog, M., 2011. Dynamics of Cdk1 Substrate Specificity during the Cell Cycle. Mol Cell 42, 610–623. https://doi.org/10.1016/j.molcel.2011.05.016

Lecuyer, E., Yoshida, H., Parthasarathy, N., Alm, C., Babak, T., Cerovina, T., Hughes, T.R., Tomancak, P., Krause, H.M., 2007. Global analysis of mRNA localization reveals a prominent role in organizing cellular architecture and function. Cell 131, 174–87. https://doi.org/10.1016/j.cell.2007.08.003

Leitao, R.M., Kellogg, D.R., 2017. The duration of mitosis and daughter cell size are modulated by nutrients in budding yeast. J Cell Biol 216, 3463–3470. https://doi.org/10.1083/jcb.201609114

Long, R.M., Chartrand, P., Gu, W., Meng, X.H., Schaefer, M.R., Singer, R.H., 1997a. Characterization of transport and localization of ASH1 mRNA in yeast. Mol Biol Cell 8, 2060–2060.

Long, R.M., Gu, W., Lorimer, E., Singer, R.H., Chartrand, P., 2000. She2p is a novel RNA-binding protein that recruits the Myo4p-She3p complex to ASH1 mRNA. Embo J 19, 6592–601. https://doi.org/10.1093/emboj/19.23.6592

Long, R.M., Singer, R.H., Meng, X., Gonzalez, I., Nasmyth, K., Jansen, R.P., 1997b. Mating type switching in yeast controlled by asymmetric localization of ASH1 mRNA. Science 277, 383–7.

Lorenz, R., Bernhart, S.H., Höner Zu Siederdissen, C., Tafer, H., Flamm, C., Stadler, P.F., Hofacker, I.L., 2011. ViennaRNA Package 2.0. Algorithms Mol Biol 6, 26. https://doi.org/10.1186/1748-7188-6-26

Lorenz, R., Hofacker, I.L., Stadler, P.F., 2016. RNA folding with hard and soft constraints. Algorithms Mol Biol 11, 8. https://doi.org/10.1186/s13015-016-0070-z

Machu, C., Eluère, R., Signon, L., Simon, M.-N., de La Roche Saint-André, C., Bailly, E., 2014. Spatially distinct functions of Clb2 in the DNA damage response. Cell Cycle 13, 383–398. https://doi.org/10.4161/cc.27354

Maekiniemi, A., Singer, R.H., Tutucci, E., 2020. Single molecule mRNA fluorescent in situ hybridization combined with immunofluorescence in S. cerevisiae: Dataset and quantification. Data in Brief 30, 105511. https://doi.org/10.1016/j.dib.2020.105511

Maher, M., Cong, F., Kindelberger, D., Nasmyth, K., Dalton, S., 1995. Cell cycle-regulated transcription of the CLB2 gene is dependent on Mcm1 and a ternary complex factor. Mol Cell Biol 15, 3129–3137.

Mueller, F., Senecal, A., Tantale, K., Marie-Nelly, H., Ly, N., Collin, O., Basyuk, E., Bertrand, E., Darzacq, X., Zimmer, C., 2013. FISH-quant: automatic counting of transcripts in 3D FISH images. Nat Methods 10, 277–8. https://doi.org/10.1038/nmeth.2406

Nevo-Dinur, K., Nussbaum-Shochat, A., Ben-Yehuda, S., Amster-Choder, O., 2011. Translation-Independent Localization of mRNA in E. coli. Science 331, 1081–1084. https://doi.org/10.1126/science.1195691

Niedner, A., Edelmann, F.T., Niessing, D., 2014. Of social molecules: The interactive assembly of ASH1 mRNA-transport complexes in yeast. RNA Biol 11, 998–1009. https://doi.org/10.4161/rna.29946

Niessing, D., Huttelmaier, S., Zenklusen, D., Singer, R.H., Burley, S.K., 2004. She2p is a novel RNA binding protein with a basic helical hairpin motif. Cell 119, 491–502. https://doi.org/10.1016/j.cell.2004.10.018

Niessing, D., Jansen, R.-P., Pohlmann, T., Feldbrügge, M., 2018. mRNA transport in fungal top models. Wiley Interdiscip Rev RNA 9. https://doi.org/10.1002/wrna.1453

Novak, B., Tyson, J.J., Gyorffy, B., Csikasz-Nagy, A., 2007. Irreversible cell-cycle transitions are due to systems-level feedback. Nat Cell Biol 9, 724–728. https://doi.org/10.1038/ncb0707-724

Olivier, C., Poirier, G., Gendron, P., Boisgontier, A., Major, F., Chartrand, P., 2005. Identification of a conserved RNA motif essential for She2p recognition and mRNA localization to the yeast bud. Mol Cell Biol 25, 4752–66. https://doi.org/10.1128/MCB.25.11.4752-4766.2005

Örd, M., Loog, M., 2019. How the cell cycle clock ticks. MBoC 30, 169–172. https://doi.org/10.1091/mbc.E18-05-0272

Paquin, N., Menade, M., Poirier, G., Donato, D., Drouet, E., Chartrand, P., 2007. Local activation of yeast ASH1 mRNA translation through phosphorylation of Khd1p by the casein kinase Yck1p. Mol Cell 26, 795–809. https://doi.org/10.1016/j.molcel.2007.05.016

Pichon, X., Robert, M.-C., Bertrand, E., Singer, R.H., Tutucci, E., 2020. New Generations of MS2 Variants and MCP Fusions to Detect Single mRNAs in Living Eukaryotic Cells. Methods Mol. Biol. 2166, 121–144. https://doi.org/10.1007/978-1-0716-0712-1_7

Raj, A., van den Bogaard, P., Rifkin, S.A., van Oudenaarden, A., Tyagi, S., 2008. Imaging individual mRNA molecules using multiple singly labeled probes. Nat Methods 5, 877–9. https://doi.org/10.1038/nmeth.1253

RColorBrewer: ColorBrewer Palettes version 1.1-2 from CRAN [WWW Document], n.d. URL https://rdrr.io/cran/RColorBrewer/ (accessed 2.4.22).

Schlichting, J.K., 2019. Modeling synchronization effects in the yeast cell cycle. http://dx.doi.org/10.18452/19835

Seiler, M., Niedner, A., Heber, S., Feldbrügge, M., Jansen, R.-P., Niessing, D., Zarnack, K., 2024. A consensus motif in ASH1 and further transcripts unifies several RNA motifs required for interaction with the She2p/She3p transport machinery and mRNA localization in yeast. https://doi.org/10.1101/2024.03.10.584336

Shahbabian, K., Jeronimo, C., Forget, A., Robert, F., Chartrand, P., 2014. Co-transcriptional recruitment of Puf6 by She2 couples translational repression to mRNA localization. Nucleic Acids Res 42, 8692–8704. https://doi.org/10.1093/nar/gku597

Shen, Z., Paquin, N., Forget, A., Chartrand, P., 2009. Nuclear shuttling of She2p couples ASH1 mRNA localization to its translational repression by recruiting Loc1p and Puf6p. Mol Biol Cell 20, 2265–75. https://doi.org/10.1091/mbc.E08-11-1151

Shepard, K.A., Gerber, A.P., Jambhekar, A., Takizawa, P.A., Brown, P.O., Herschlag, D., DeRisi, J.L., Vale, R.D., 2003. Widespread cytoplasmic mRNA transport in yeast: Identification of

22 bud-localized transcripts using DNA microarray analysis. PNAS 100, 11429–11434. https://doi.org/10.1073/pnas.2033246100

Soifer, I., Barkai, N., 2014. Systematic identification of cell size regulators in budding yeast. Mol Syst Biol 10, 761. https://doi.org/10.15252/msb.20145345

Spellman, P.T., Sherlock, G., Zhang, M.Q., Iyer, V.R., Anders, K., Eisen, M.B., Brown, P.O., Botstein, D., Futcher, B., 1998. Comprehensive Identification of Cell Cycle–regulated Genes of the Yeast Saccharomyces cerevisiae by Microarray Hybridization. Mol Biol Cell 9, 3273–3297.

Spiesser, T.W., Kühn, C., Krantz, M., Klipp, E., 2015. Bud-Localization of CLB2 mRNA Can Constitute a Growth Rate Dependent Daughter Sizer. PLOS Computational Biology 11, e1004223. https://doi.org/10.1371/journal.pcbi.1004223

Spiesser, T.W., Müller, C., Schreiber, G., Krantz, M., Klipp, E., 2012. Size homeostasis can be intrinsic to growing cell populations and explained without size sensing or signalling. FEBS J 279, 4213–4230. https://doi.org/10.1111/febs.12014

Sprouffske, K., Wagner, A., 2016. Growthcurver: an R package for obtaining interpretable metrics from microbial growth curves. BMC Bioinformatics 17, 172. https://doi.org/10.1186/s12859-016-1016-7

Stern, B., Nurse, P., 1996. A quantitative model for the cdc2 control of S phase and mitosis in fission yeast. Trends in Genetics 12, 345–350. https://doi.org/10.1016/S0168-9525(96)80016-3

Stueland, M., Wang, T., Park, H.Y., Mili, S., 2019. RDI Calculator: An Analysis Tool to Assess RNA Distributions in Cells. Sci Rep 9, 1–10. https://doi.org/10.1038/s41598-019-44783-2

Surana, U., Amon, A., Dowzer, C., McGrew, J., Byers, B., Nasmyth, K., 1993. Destruction of the CDC28/CLB mitotic kinase is not required for the metaphase to anaphase transition in budding yeast. The EMBO journal 12, 1969–78.

Surana, U., Robitsch, H., Price, C., Schuster, T., Fitch, I., Futcher, A.B., Nasmyth, K., 1991. The role of CDC28 and cyclins during mitosis in the budding yeast S. cerevisiae. Cell 65, 145–161. https://doi.org/10.1016/0092-8674(91)90416-v

Takizawa, P.A., Vale, R.D., 2000. The myosin motor, Myo4p, binds Ash1 mRNA via the adapter protein, She3p. Proc Natl Acad Sci U S A 97, 5273–8. https://doi.org/10.1073/pnas.080585897

Talia, S.D., Skotheim, J.M., Bean, J.M., Siggia, E.D., Cross, F.R., 2007. The effects of molecular noise and size control on variability in the budding yeast cell cycle. Nature 448, 947–951. https://doi.org/10.1038/nature06072

Trcek, T., Larson, D.R., Moldon, A., Query, C.C., Singer, R.H., 2011. Single-Molecule mRNA Decay Measurements Reveal Promoter-Regulated mRNA Stability in Yeast. Cell 147, 1484–1497. https://doi.org/10.1016/j.cell.2011.11.051

Tutucci, E., Livingston, N.M., Singer, R.H., Wu, B., 2018a. Imaging mRNA in vivo, from Birth to Death. Annu Rev Biophys 47. https://doi.org/10.1146/annurev-biophys-070317-033037

Tutucci, E., Singer, R.H., 2020. Simultaneous Detection of mRNA and Protein in S. cerevisiae by Single-Molecule FISH and Immunofluorescence. Methods Mol. Biol. 2166, 51–69. https://doi.org/10.1007/978-1-0716-0712-1_4

Tutucci, E., Vera, M., Biswas, J., Garcia, J., Parker, R., Singer, R.H., 2018b. An improved MS2 system for accurate reporting of the mRNA life cycle. Nat Methods 15, 81–89. https://doi.org/10.1038/nmeth.4502

Tutucci, E., Vera, M., Singer, R.H., 2018c. Single-mRNA detection in living S. cerevisiae using a re-engineered MS2 system. Nat Protoc 13, 2268–2296. https://doi.org/10.1038/s41596-018-0037-2

Veis, J., Klug, H., Koranda, M., Ammerer, G., 2007. Activation of the G2/M-specific gene CLB2 requires multiple cell cycle signals. Molecular and cellular biology 27, 8364–73. https://doi.org/10.1128/MCB.01253-07

Visintin, R., Amon, A., 2001. Regulation of the mitotic exit protein kinases Cdc15 and Dbf2. Molecular biology of the cell 12, 2961–74.

Wanless, A.G., Lin, Y., Weiss, E.L., 2014. Cell Morphogenesis Proteins Are Translationally Controlled through UTRs by the Ndr/LATS Target Ssd1. PLOS ONE 9, e85212. https://doi.org/10.1371/journal.pone.0085212

Wickham, H., 2016. ggplot2: Elegant Graphics for Data Analysis, 2nd ed, Use R! Springer International Publishing. https://doi.org/10.1007/978-3-319-24277-4

Wickham, H., Averick, M., Bryan, J., Chang, W., McGowan, L.D., François, R., Grolemund, G., Hayes, A., Henry, L., Hester, J., Kuhn, M., Pedersen, T.L., Miller, E., Bache, S.M., Müller, K., Ooms, J., Robinson, D., Seidel, D.P., Spinu, V., Takahashi, K., Vaughan, D., Wilke, C., Woo, K., Yutani, H., 2019. Welcome to the Tidyverse. Journal of Open Source Software 4, 1686. https://doi.org/10.21105/joss.01686

Yang, X., Jost, A.P.-T., Weiner, O.D., Tang, C., 2013. A light-inducible organelle-targeting system for dynamically activating and inactivating signaling in budding yeast. MBoC 24, 2419–2430. https://doi.org/10.1091/mbc.e13-03-0126

Zenklusen, D., Larson, D.R., Singer, R.H., 2008. Single-RNA counting reveals alternative modes of gene expression in yeast. Nat Struct Mol Biol 15, 1263–71. https://doi.org/10.1038/nsmb.1514

Zhu, G., Spellman, P.T., Volpe, T., Brown, P.O., Botstein, D., Davis, T.N., Futcher, B., 2000. Two yeast forkhead genes regulate the cell cycle and pseudohyphal growth. Nature 406, 90–94. https://doi.org/10.1038/35017581

Figure 1

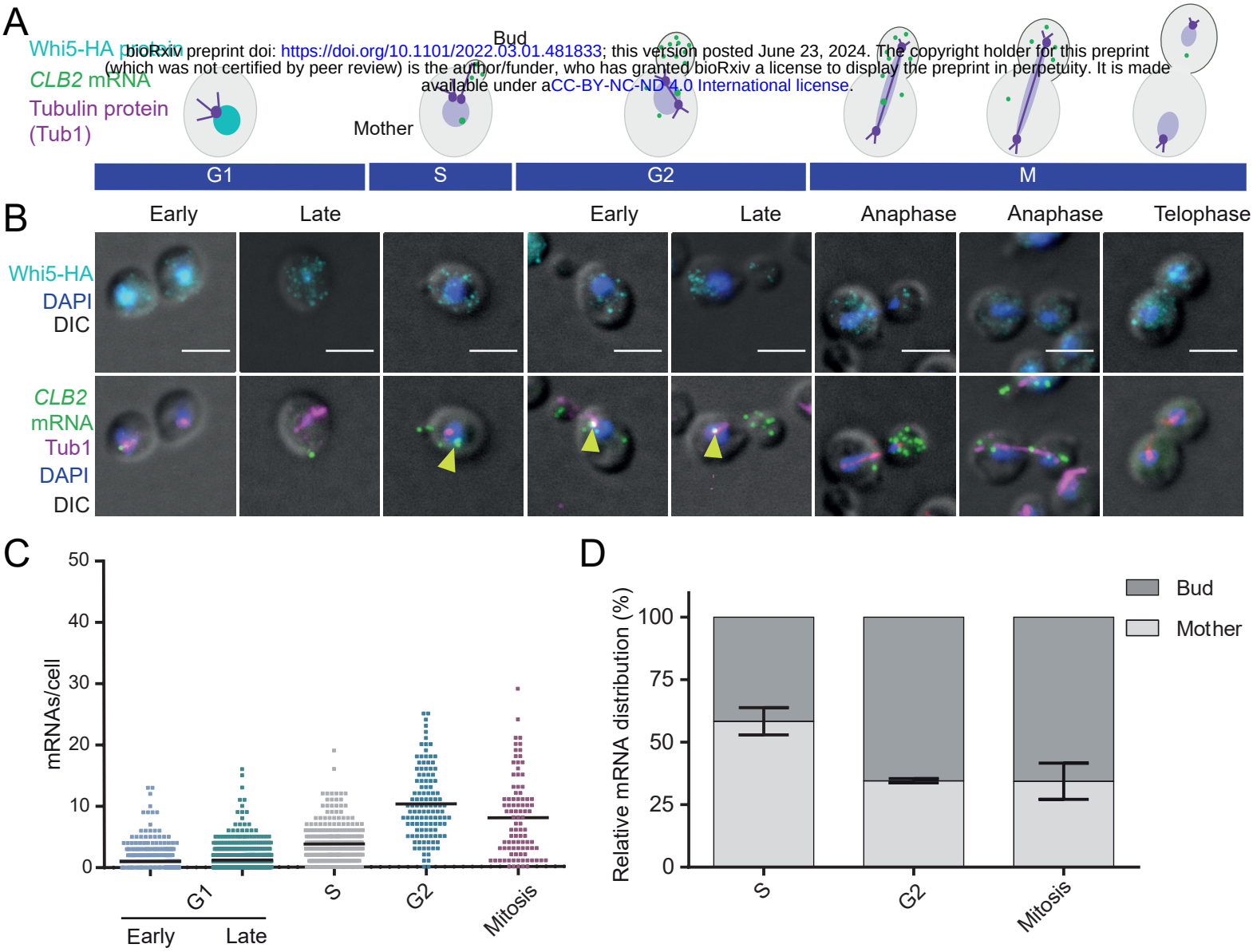

Figure 2

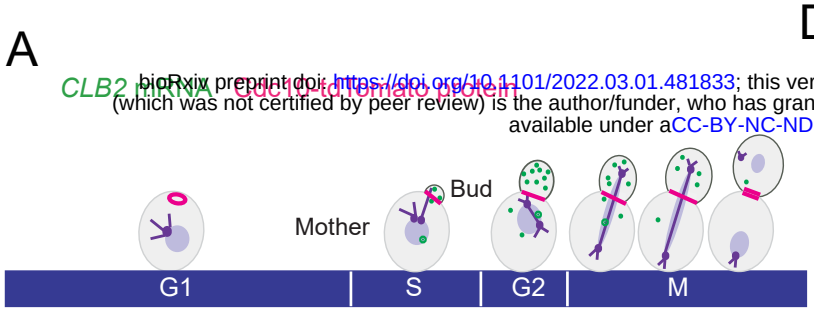

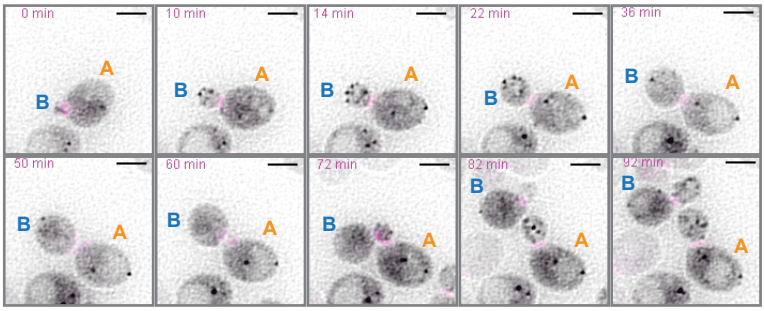

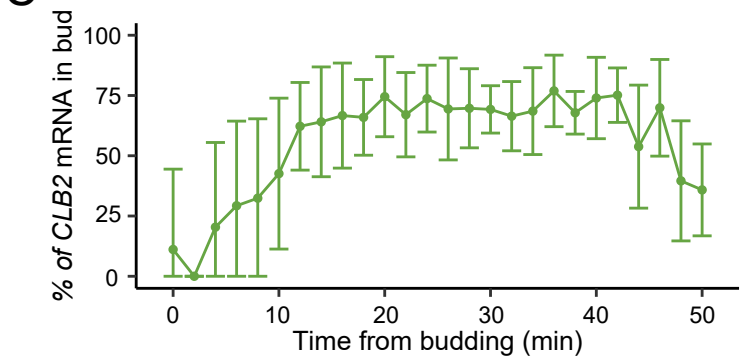

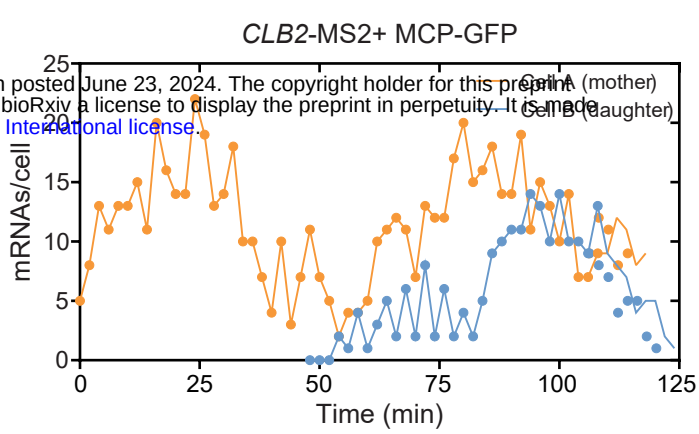

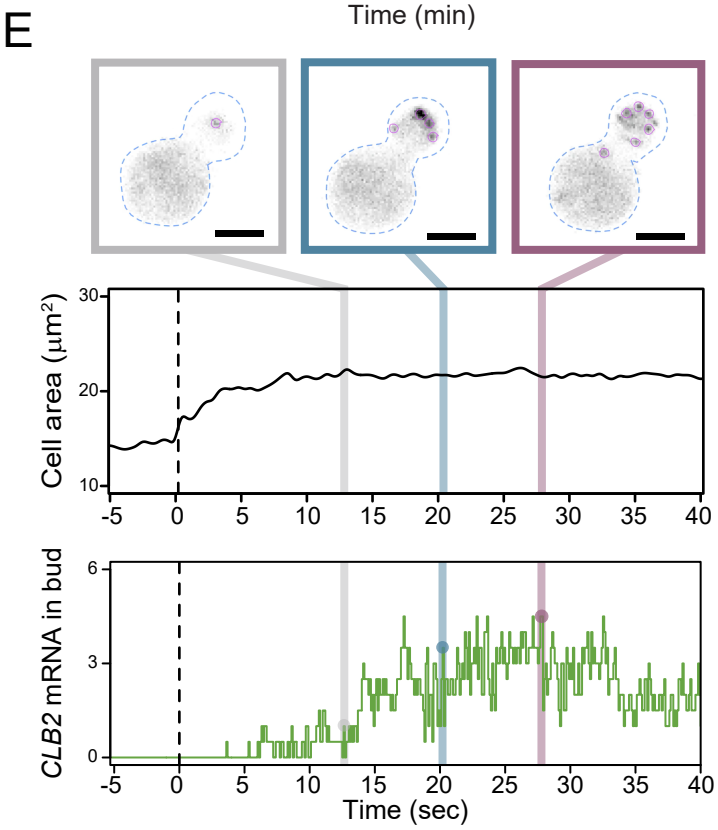

Figure 3

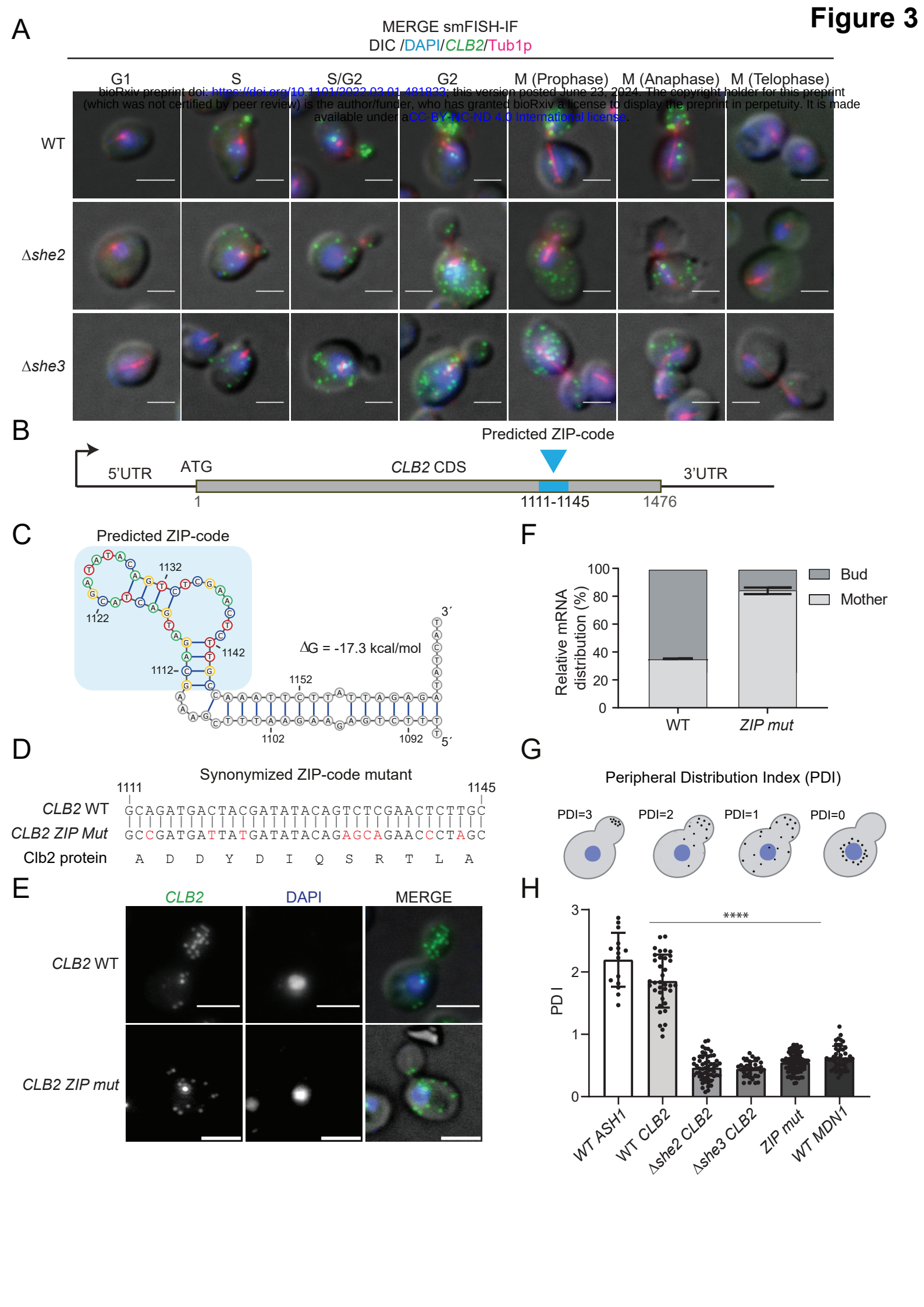

Figure 4

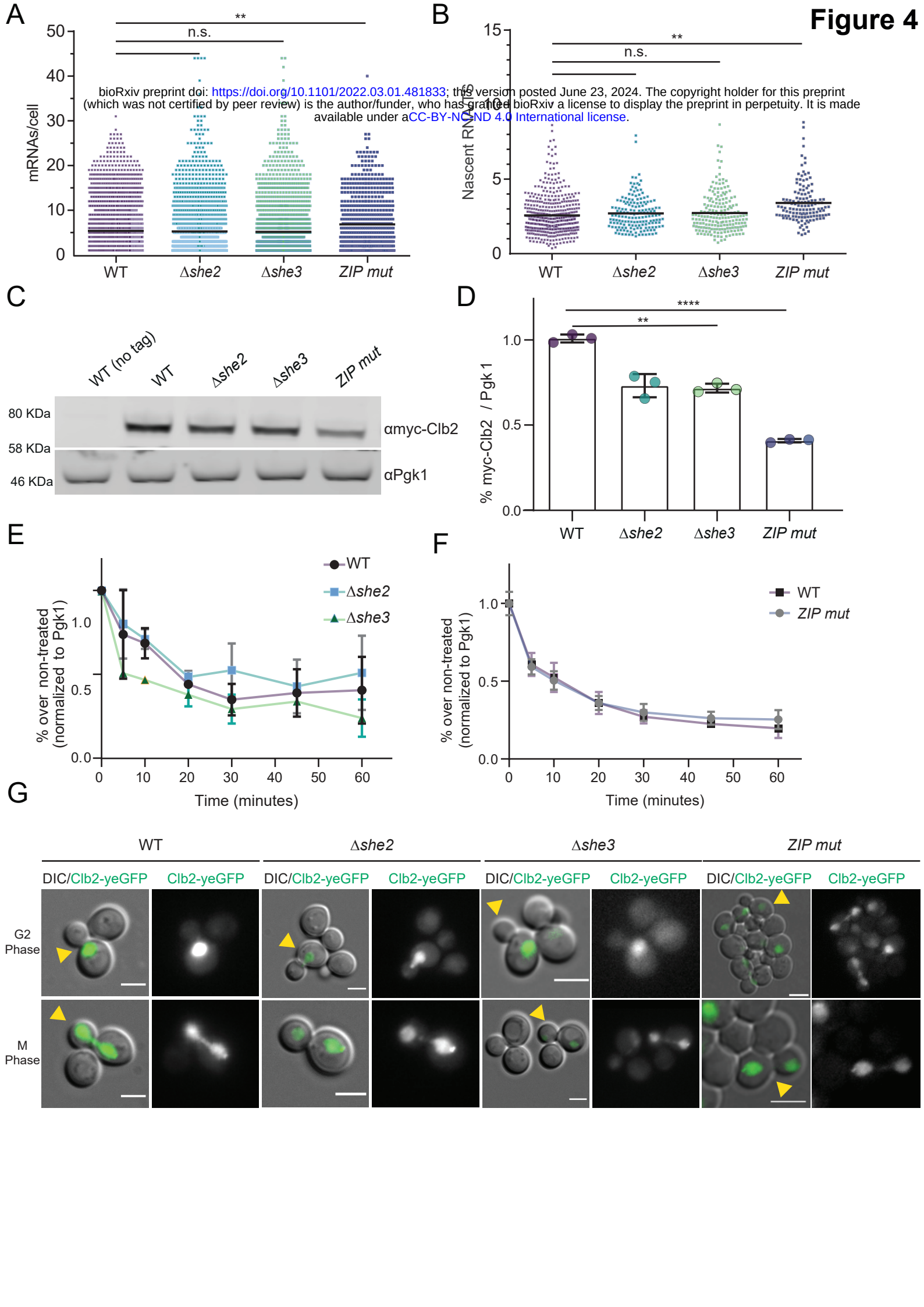

Figure 5

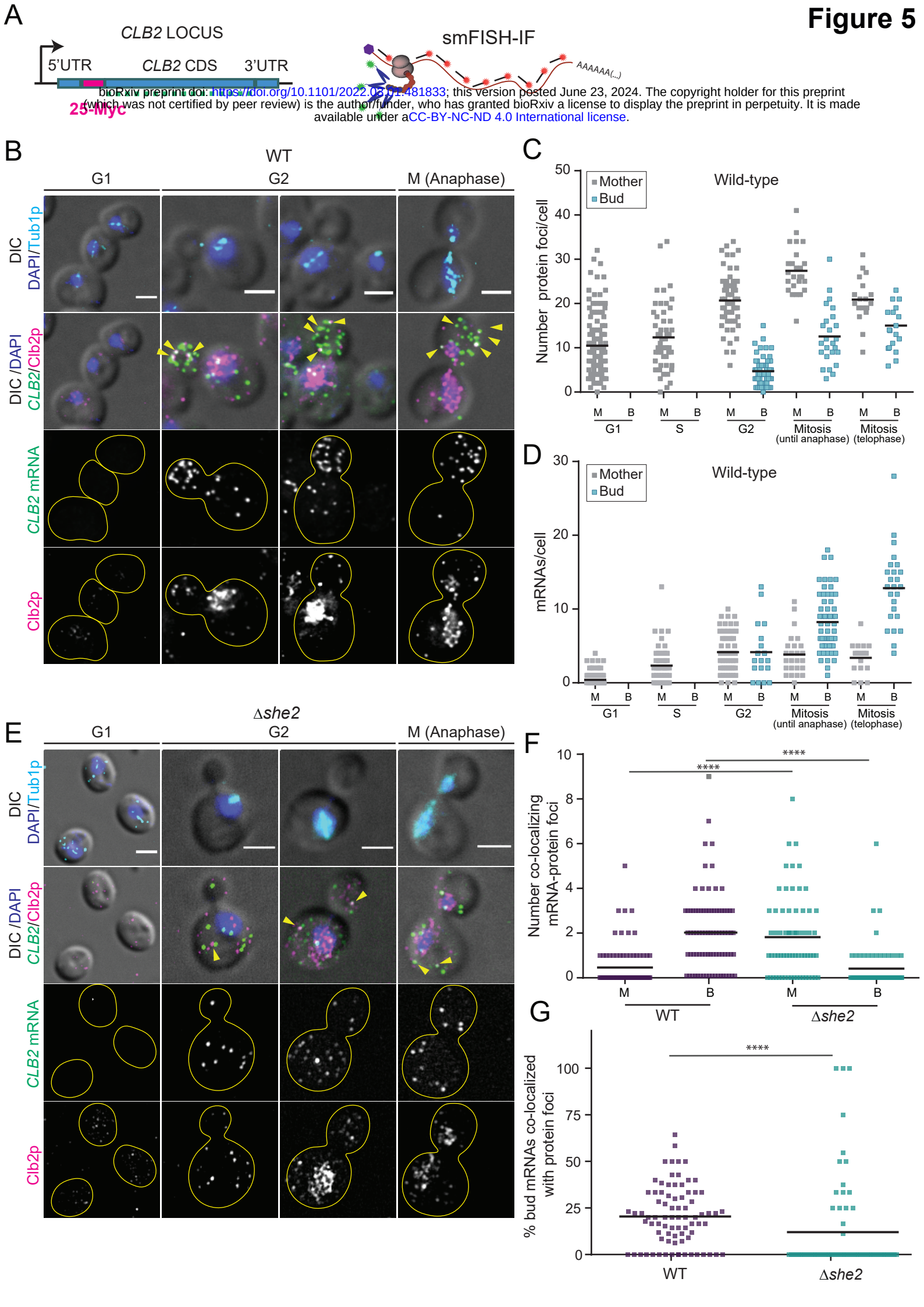

Figure 6

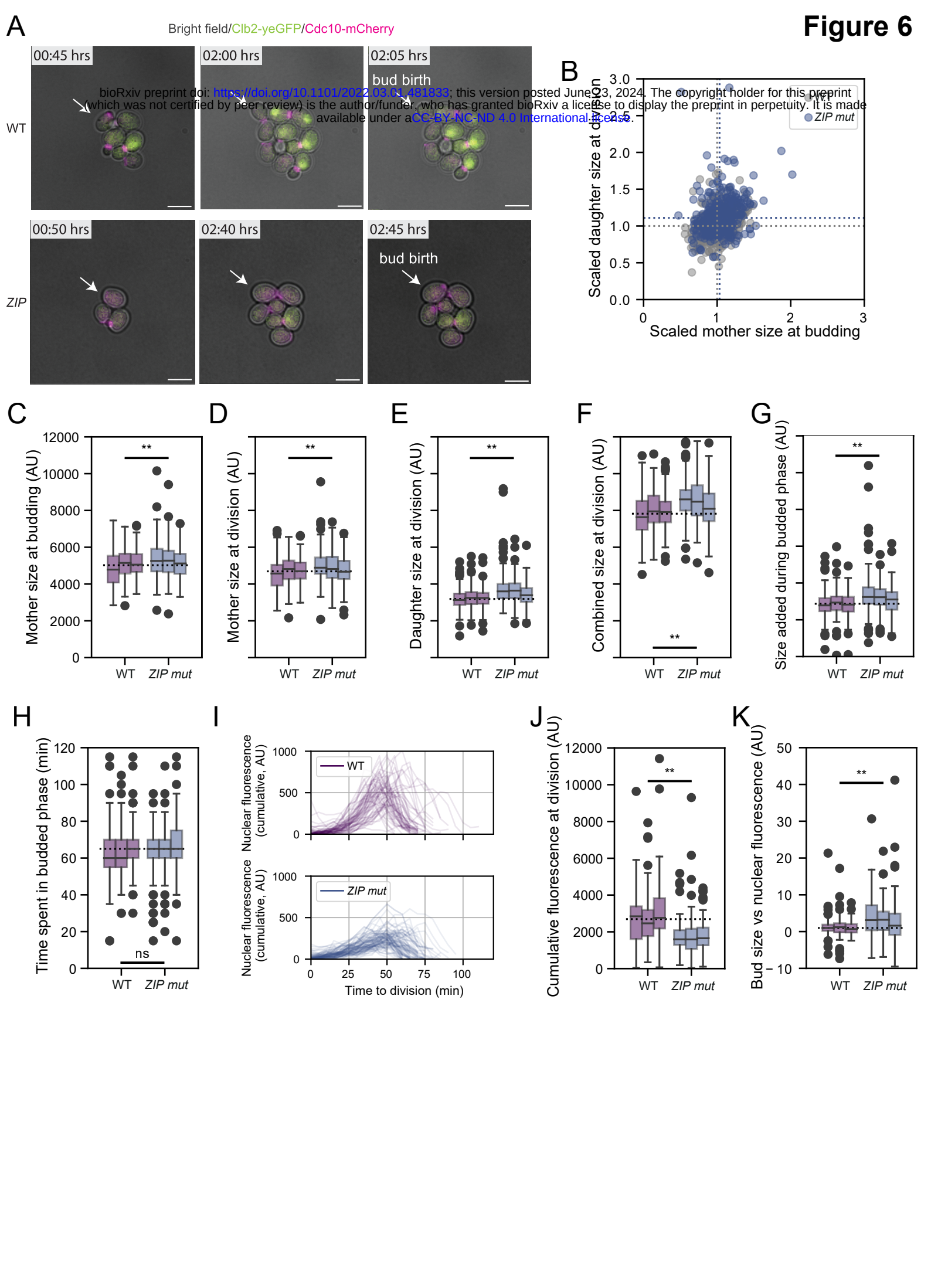

Figure 7

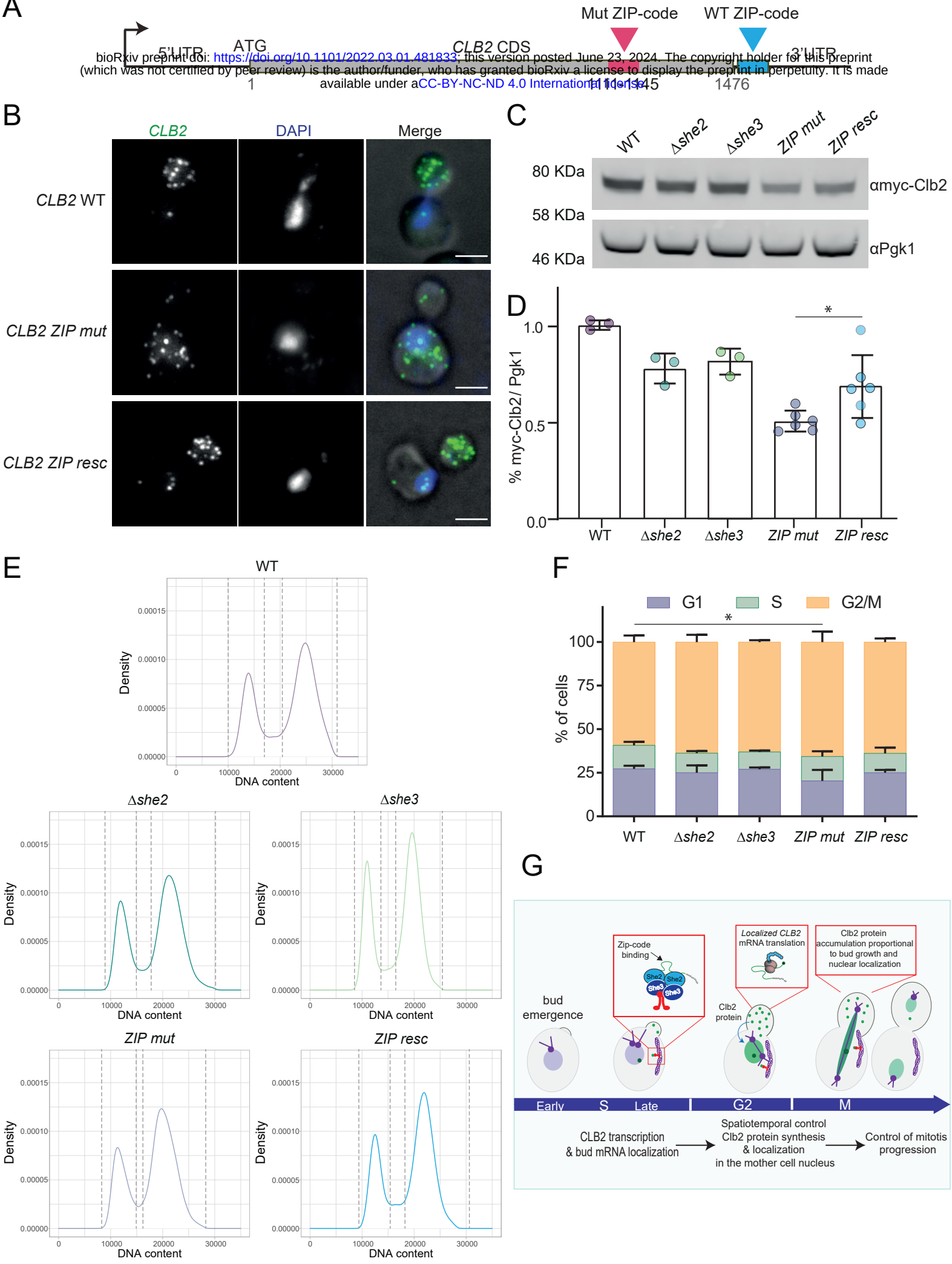

Figure S1

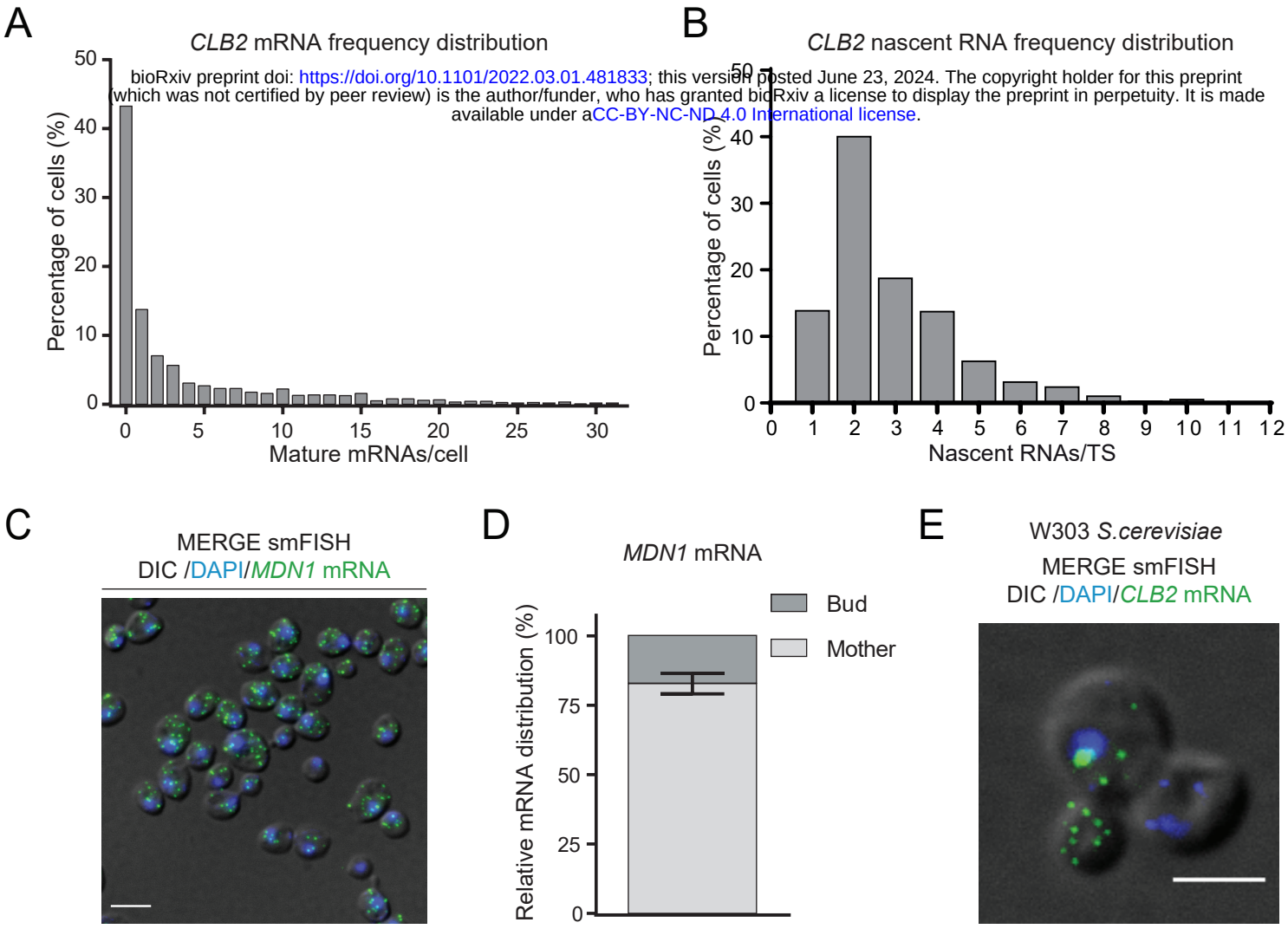

Figure S2

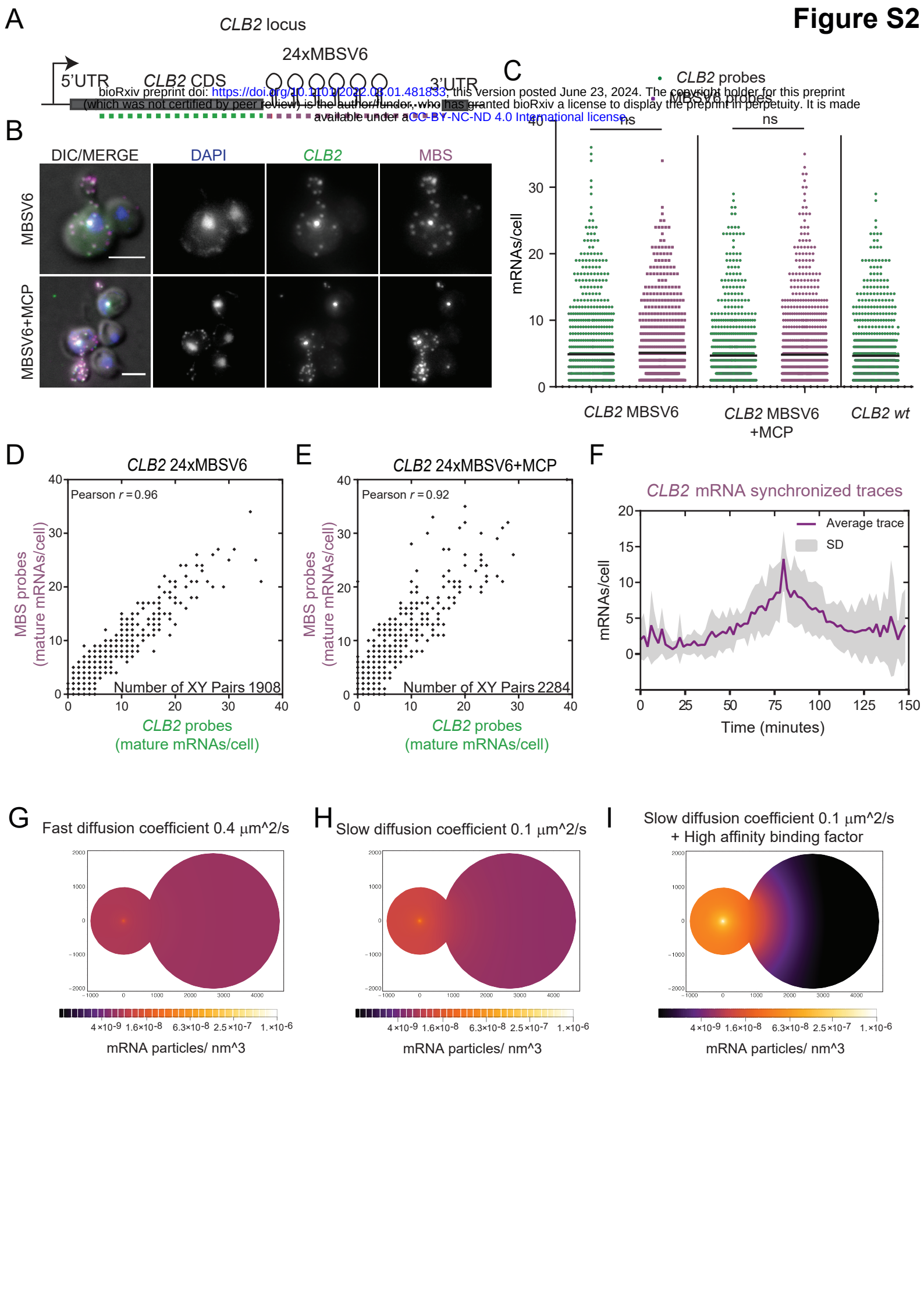

Figure S3

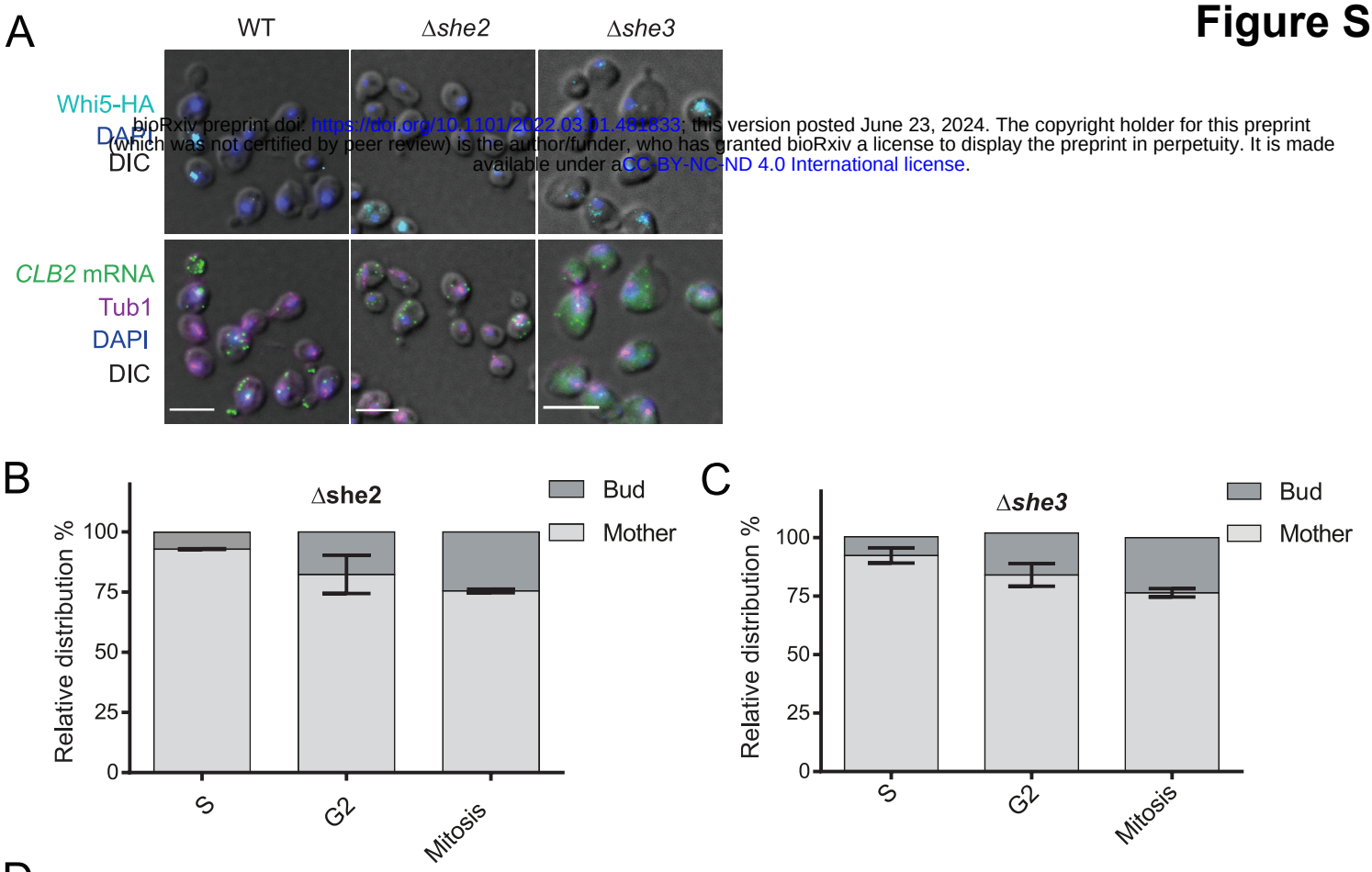

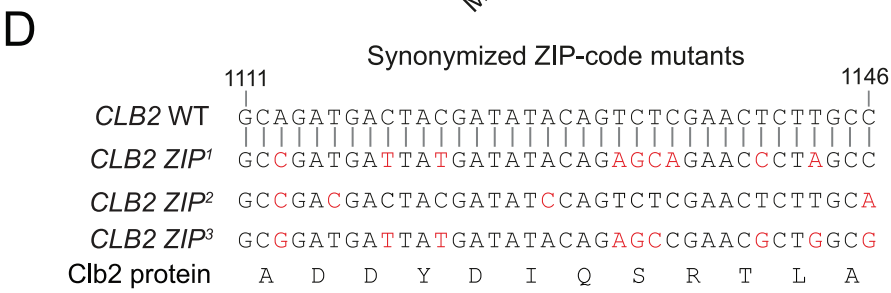

E

Strain	Amino acid seq A	D	D	Y	D	I	Q	S	R	T	L	A	Average
WT	0.29	0.65	0.35	0.44	0.65	0.56	0.31	0.26	0.07	0.35	0.13	0.22	0.36
ZIP1	0.22	0.65	0.65	0.56	0.65	0.56	0.31	0.11	0.48	0.22	0.14	0.22	0.40
ZIP2	0.22	0.35	0.35	0.44	0.65	0.26	0.31	0.26	0.07	0.35	0.13	0.38	0.31
ZIP3	0.11	0.65	0.65	0.56	0.65	0.56	0.31	0.11	0.07	0.13	0.11	0.11	0.34

Codon usage freq

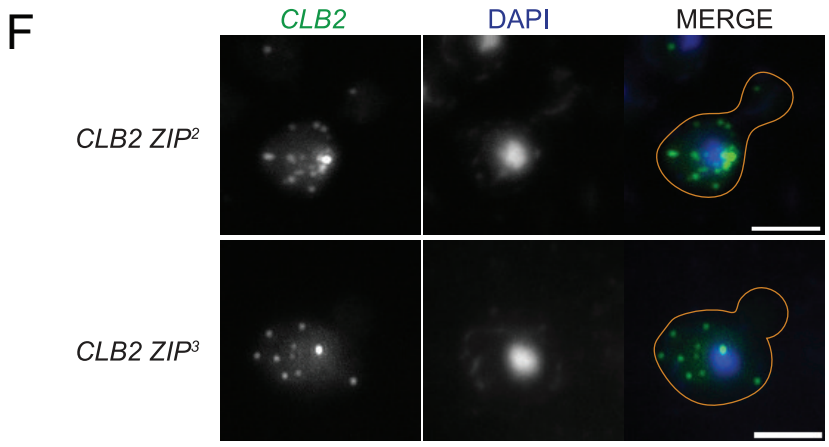

Figure S4

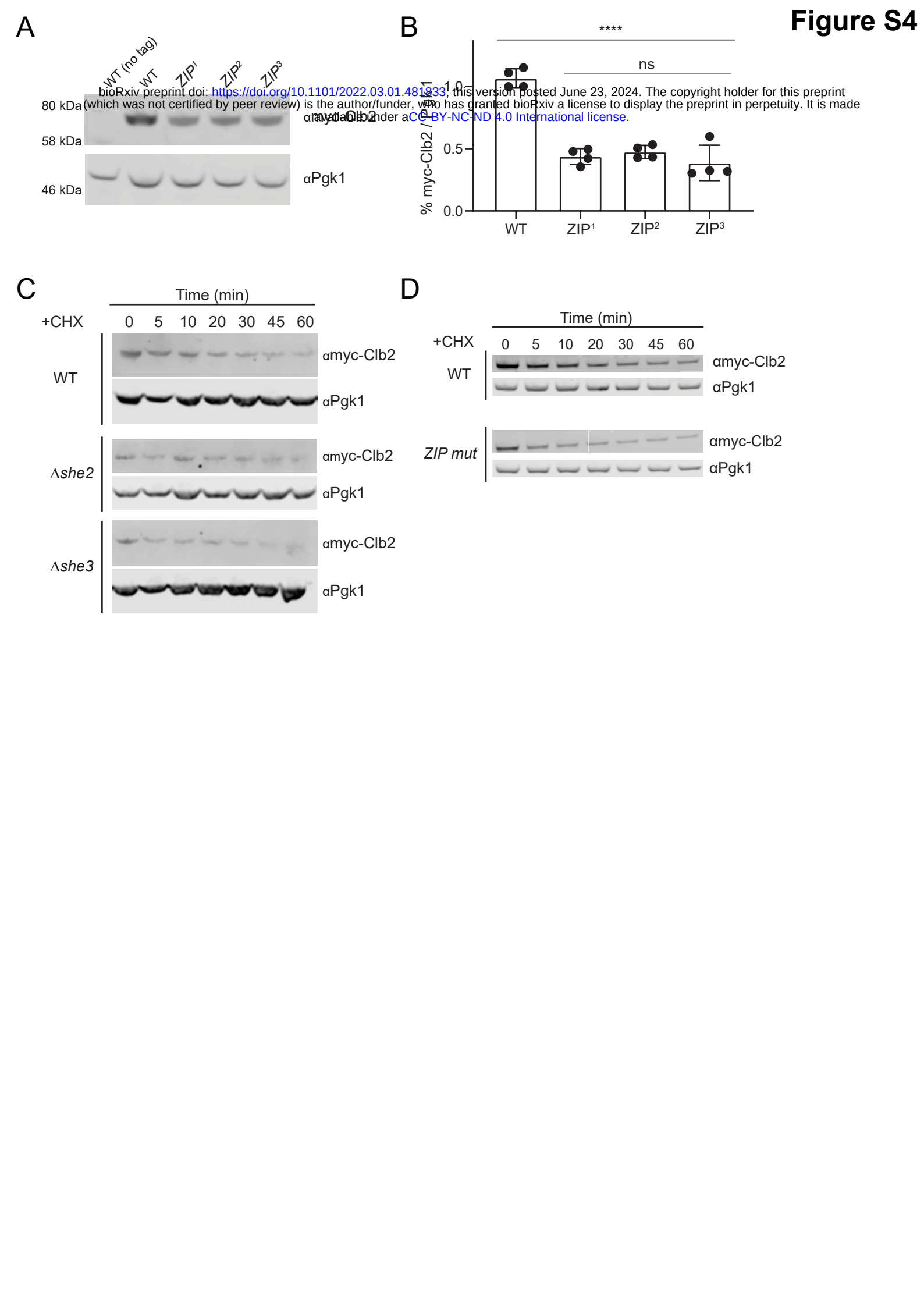

Figure S5

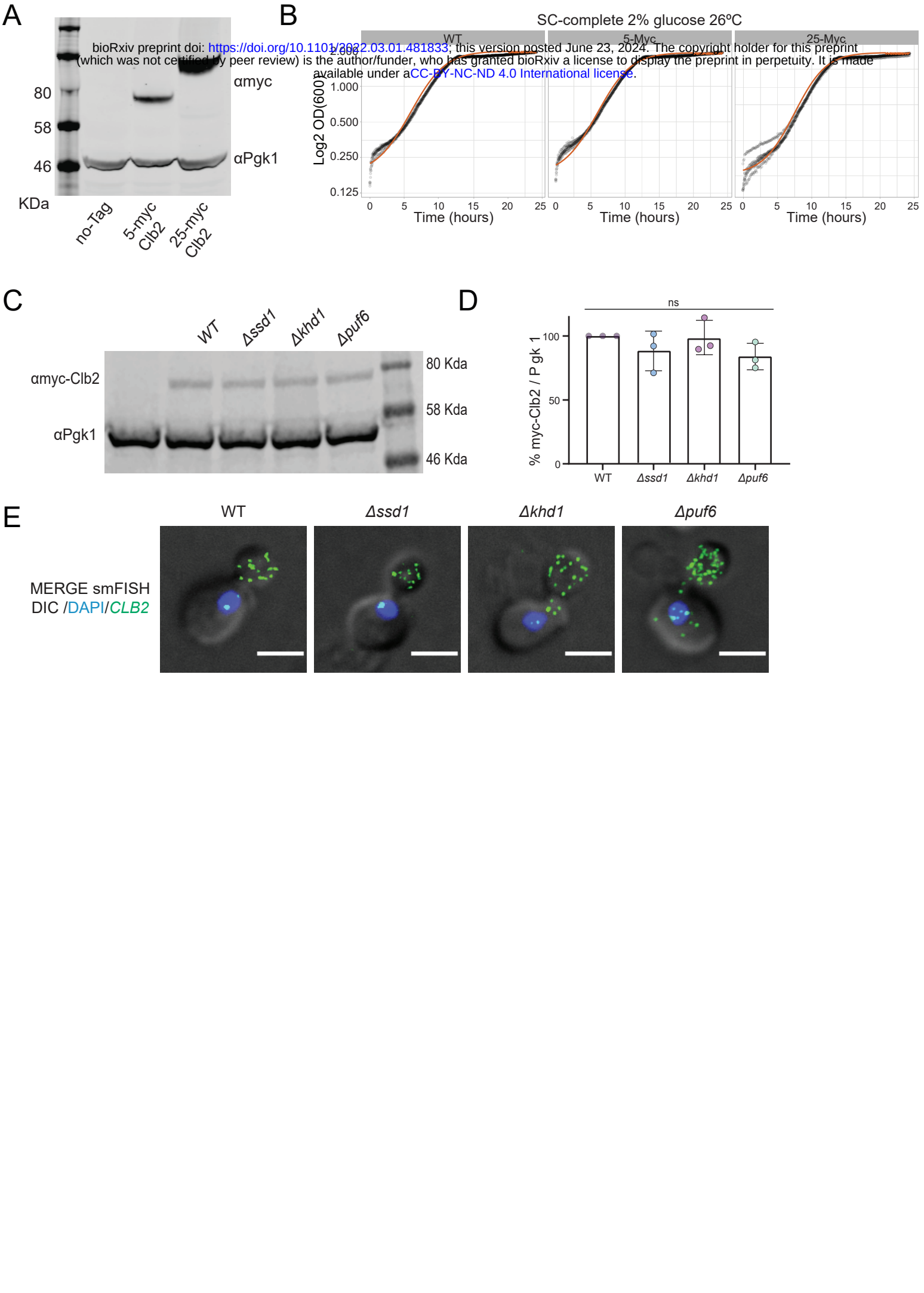

Figure S6

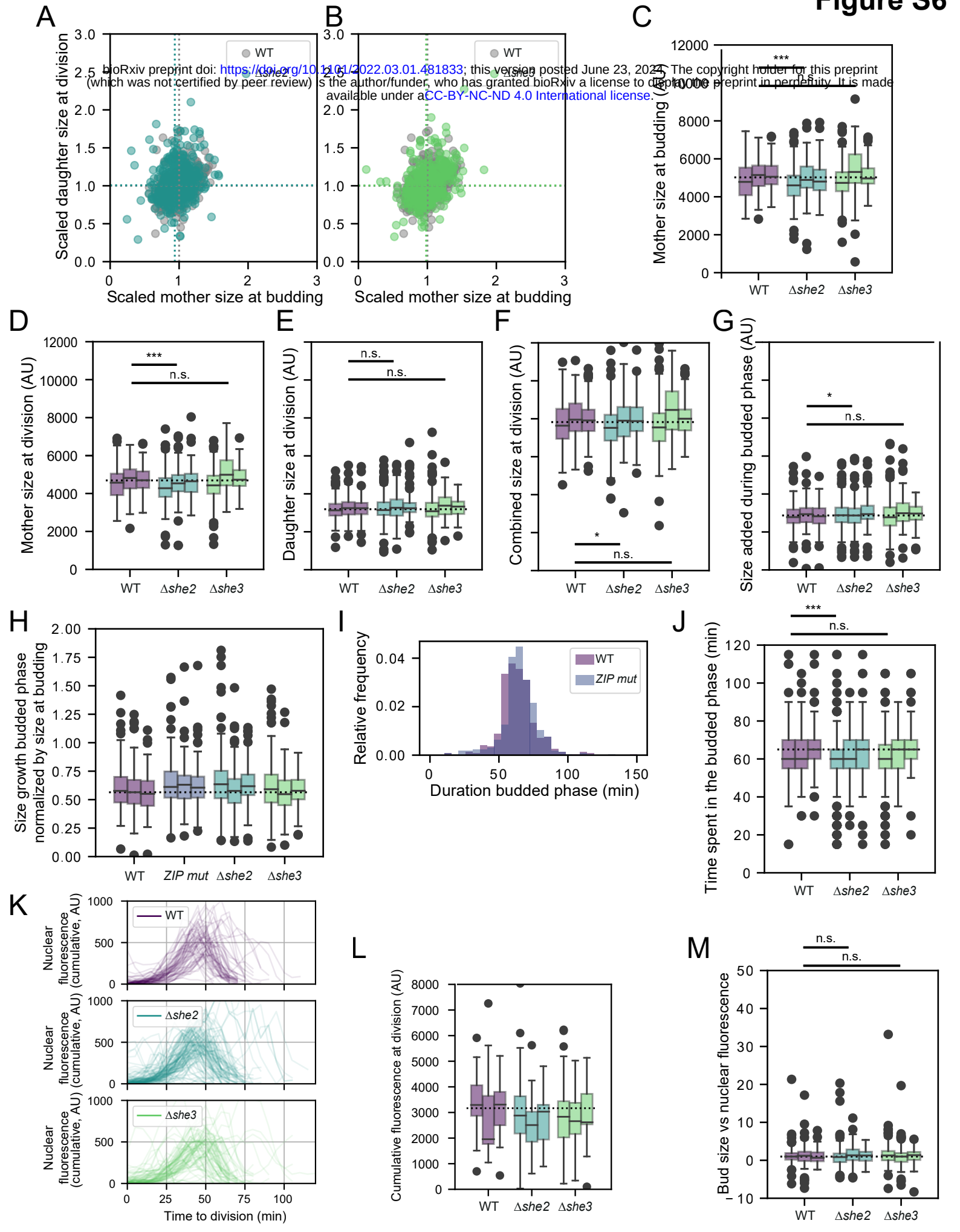

Figure S7